JOURNAL OF GEOPHYSICAL RESEARCH, VOL. 105, NO. C1, PAGES 1245–1269, JANUARY 15, 2000

Spatial and temporal characteristics of the mesoscale circulation of the California Current from eddy-resolving moored and shipboard measurements

T. K. Chereskin,[1] M. Y. Morris,[1,2] P. P. Niiler,[1] P. M. Kosro,[3] R. L. Smith,[3] S. R. Ramp,[4] C. A. Collins,[4] and D. L. Musgrave[5]

Abstract. Moored observations of currents and temperatures made in the upper 600 m on eddy-resolving scales over a 2-year period are used to examine the spatial and temporal characteristics of the California Current mesoscale circulation. The observations were made at three principal longitudes: 124°W, 126°W, and 128°W in the vicinity of Point Arena. They bracket the 600-km-wide band of high mesoscale variability found along the eastern boundary of the North Pacific. At all locations, the mesoscale variability was larger than the mean flow, and the spatial modes of variability as determined from empirical orthogonal function analysis consisted of an alongshore mode, a cross-shore mode, and a rotational mode. Observations made near the continental slope (124°W) were dominated by the poleward flowing California Undercurrent, with mesoscale eddies and meanders superposed. The nearshore eddy kinetic energy peaked in a band centered around 60 days. Observations made at 128°W, near the offshore boundary between the energetic mesoscale band and the "eddy desert" of the northeast Pacific, were characterized by small means, fewer eddy events, and a peak in eddy kinetic energy at 120-180 days. The good horizontal resolution of the current meter arrays allowed us to estimate the relative vorticity, horizontal divergence, and Rossby number and therefore to evaluate the relative strength and occurrence of anticyclones and cyclones. We found the mesoscale eddy field to be strongly nonlinear, with Rossby numbers ranging from 0.1 to 0.5. All of the eddies observed at the offshore site were nonlinear, deep, warm anticyclones. Shipboard hydrography revealed the origin of one of these anticyclones to be the California Undercurrent, and this eddy retained its strong anomalies after several months and several hundred kilometers of propagation. Despite the lower incidence of eddies as one moves west from the coast, the eddies that we observed offshore provide evidence for propagation and transport of properties from the coast to the central North Pacific across the California Current System.

1. Introduction

From hydrographic surveys, satellite observations [*Strub et al.*, 1997; *Kelly et al.*, 1998; *Strub and James*, 1999], and surface drifter measurements (Plate 1), it is clear that a field of vigorous mesoscale eddies exists in the California Current System (CCS), extending from Oregon to Baja California, and from the coast to about 600 km offshore. While the CCS is one of the most intensively surveyed regions of the world's oceans (beginning with Harold Sverdrup in 1937), most of the historical data have insufficient spatial and temporal sampling to resolve the mesoscale. Some notable exceptions are eddy-resolving surveys off both southern and northern California [e.g., *Simpson and Lynn*, 1990; *Walstad et al.*, 1991; *Rienecker and Mooers*, 1989]. An important conclusion of these studies is that eddies were observed to penetrate to about 800 m, well below the main thermocline depth which contains the bulk of the quasi-geostrophic mean flow. The amplitude of these eddies (dynamic height anomaly of 0.15 dyn. m) can be as large as the total steric height increase across the California Current, and hence the southward flow of the CCS can be, and often is, disrupted by these strong mesoscale features. Another important aspect of strong eddies is that they can trap anomalous fluid at depth. Their propagation in the CCS is generally westward, perpendicular to the mean flow. Hence, in addition to influencing the circulation, they play a potentially important role in transport and mixing, one that is orthogonal to the mean and often over greater depth range. There is apparently a

[1] Scripps Institution of Oceanography, University of California, San Diego.

[2] Now at National Institute of Water and Atmospheric Research Ltd., Wellington, New Zealand.

[3] Oregon State University, Corvallis.

[4] Department of Oceanography, Naval Postgraduate School, Monterey, California.

[5] Institute of Marine Science, University of Alaska, Fairbanks.

Paper number 1999JC900252.
0148-0227/00/1999JC900252$09.00

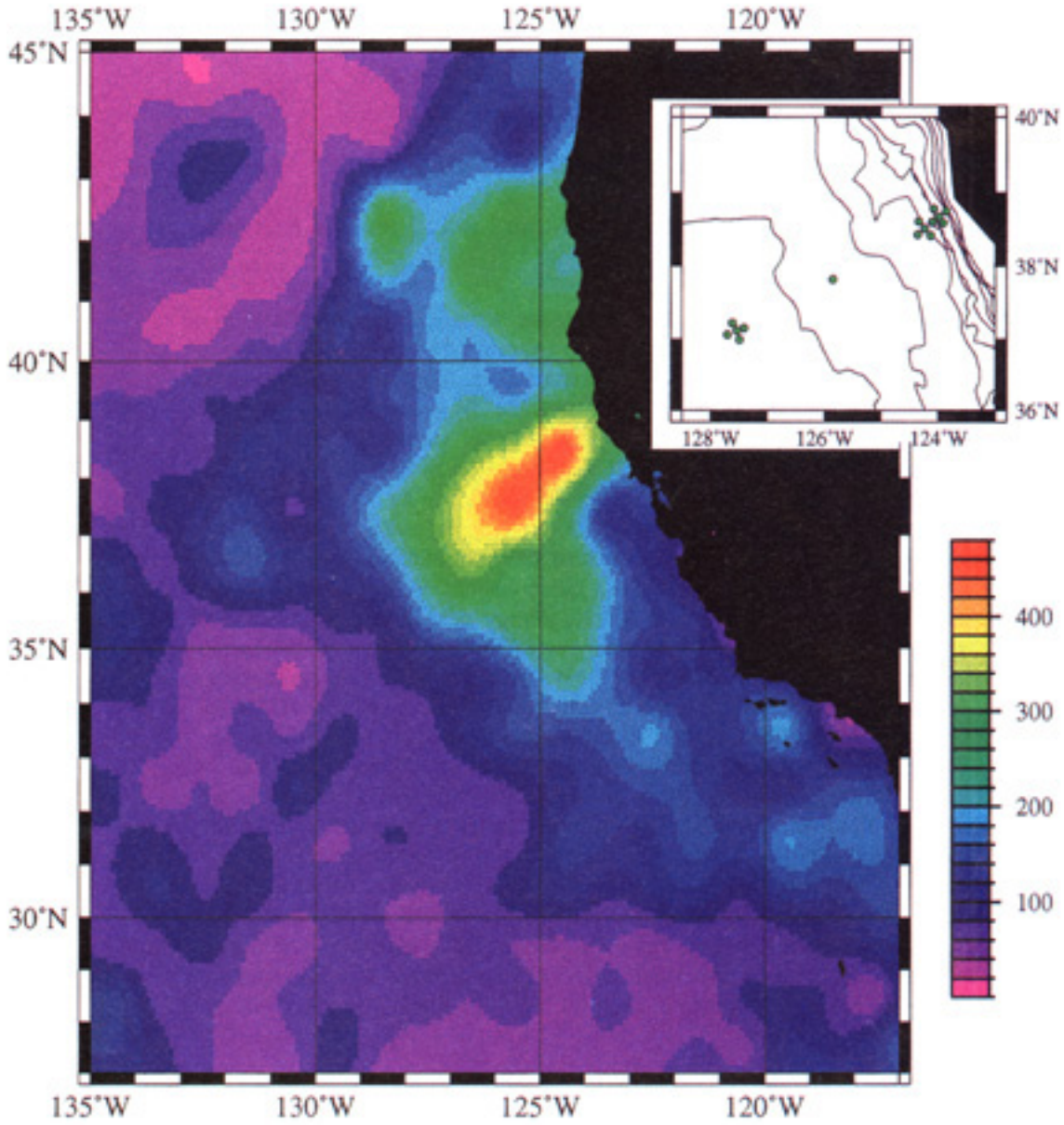

Plate 1. Surface eddy kinetic energy (cm^2s^{-2}) reveals a high-variability band that extends from the coast to about 600 km offshore, from Oregon to Baja California. Eddy kinetic energy was calculated from spatially binned (1°x 1°), 2-day-averaged velocities at 15-m depth measured by surface drifters during the period from November 1985 until September 1998. The basic drifter data set was quality-controlled, interpolated, and compiled by the Drifter Data Assembly Center at NOAA/AOML [*Hansen and Poulain*, 1996]. The inset shows the bathymetry (contours every 500 m, from 500 to 4500 m) and the locations of the 15 moorings (green-filled circles) that comprise the California Current moored array (CCMA). Note that the moorings bracket the particularly high variability band off Point Arena, California.

seasonal cycle to the generation and westward propagation of the mesoscale eddy field, with an intensification of the eddy energy at the coast during the spring and summer upwelling season [e.g., *Kelly et al.*, 1998].

In 1992–1994, the Office of Naval Research sponsored a major field program (Eastern Boundary Currents, or EBC) to study interactions in nonlinear mesoscale regimes such as the CCS, which included current meter moorings [*Ramp et al.*, 1994; *Kosro et al.*, 1994; *Chereskin*, 1995], surveys [*Huyer et al.*, 1998; *Shearman et al.*, 1999], surface drifter measurements [*Kelly et al.*, 1998], subsurface floats [*Collins et al.*, 1996; *Garfield et al.*, 1999], and satellite observations [*Strub et al.*, 1997; *Kelly et al.*, 1998]. In this paper, we describe and compare mesoscale variability from the EBC moored observations, which were made on eddy-resolving scales at the inshore (124°W) and offshore (128°W) limits of the band of high mesoscale variability in the vicinity of Point Arena, California (Plate 1, inset). One goal of EBC was to extend ocean mesoscale observations of the California Current geographically and temporally from previous measurements made during spring and summer on the continental shelf and slope out into deep water and over two

annual cycles. Additionally, the moorings were designated as the World Ocean Circulation Experiment (WOCE) PCM2 array, and the WOCE hydrographic survey line P17N sampled past the moored arrays in May 1993 [*Musgrave and Royer*, 1994].

Although currents on the continental shelf and slope off of northern California have been densely sampled in experiments such as the Northern California Coastal Currents Study (NCCCS), the Coastal Ocean Dynamics Experiment (CODE), and other studies [e.g., *Winant et al.*, 1987; *Largier et al.*, 1993; *Ramp et al.*, 1997], there are relatively few long records of moored currents offshore of the continental slope. Most of what is known about the circulation offshore of the continental margin has been inferred from geostrophic calculations [*Wyllie*, 1966; *Hickey*, 1979; *Lynn and Simpson*, 1987] and, more recently, from surface drifter observations (Plate 1). *Stabeno and Smith* [1987] present a synthesis of 14 current meter records at eight deep-sea locations off of Point Arena. Most of the records are 1 year in length (one is 5 years), and the horizontal separation between moorings is large (> 50 km). The EBC time series (15 moorings, 2 years; one is 4 years) roughly triple the moored observations of ocean currents over deep water. These long records are particularly useful at the offshore site (128°W), where the integral timescales [*Davis*, 1976] are long, O(20 days). Additionally, the horizontal separation within the EBC moored arrays (15 km) was roughly half the local internal Rossby deformation radius, allowing mesoscale features to be resolved.

In the following sections, we present a basic description of the low-frequency mesoscale variability observed over the entire 2-year time period, 1992–1994. A detailed analysis and model of a nonlinear eddy observed at the offshore array at the time of the WOCE survey is the topic of a separate study [*Cornuelle et al.*, this issue]. The observations are presented in section 2, followed by a statistical description in section 3. We then examine the spatial modes of variability through empirical orthogonal function (EOF) analysis in section 4. Individual eddy events and kinematic and dynamical balances are presented in section 5. A summary and conclusions are presented in section 6.

2. Data

2.1. California Current Moored Array

The California Current moored array (CCMA) consisted of three eddy-resolving, spatially coherent subarrays called local dynamics arrays (LDAs). Each LDA was composed of five moorings: four moorings forming a square around a central mooring, with a horizontal separation of 15 km. The LDA located at 128°W was designated as the offshore LDA (moorings labeled OW, OS, ON, OC, OE). The central mooring at the offshore site (OC) was located under a Topex crossover point [*Strub et al.*, 1997] and was adjacent to a densely instrumented surface buoy [*Chereskin*, 1995]; it was maintained for 4 years as part of an acoustic source array [*Garfield et al.*, 1999]. The remaining two LDAs, collectively referred to as the nearshore arrays, spanned the continental slope and the deep water adjacent to the slope near 124°W. The slope LDA (moorings labeled MW, MS, MN, MC, ME) was centered on the 2000-m isobath. It shared a vertex (mooring MW = IE) with the inshore LDA (moorings labeled IW, IS, IN, IC), so named because it was located on the inshore side of the California Current. The original CCMA plan included a line of moorings between the offshore and inshore sites. Resources were insufficient to deploy the line, but a single mooring (labeled IOC) was deployed roughly at the midpoint to provide statistics at a mid–California Current location.

Measurements were obtained for a 2-year period beginning in boreal summer 1992 at four target depths: 100 m, 150 m, 300 m, and 600 m. The year runs from June for the slope LDA and from August for the inshore and offshore LDAs. Mooring locations, water depths, actual instrument depths, record lengths, and current meter types are given in Table 1.

2.2. Data Processing

Four different types of current meters were used (Table 1), and all types perform well on subsurface moorings provided that the instruments and flotation are well beneath the surface gravity wave zone, as was the case for these deployments. The VACM, acoustic Doppler current profiler (ADCP), and RCM8 are all vector-averaging current meters. The RCM5 averages current magnitude and instantaneously samples direction at the end of the averaging interval. Comparisons of statistics between instruments at common depths (Table 2) indicates that the differences between instrument types were negligible, at least for the low-pass-filtered, low-frequency variability. For direct comparison, we placed an RCM5/VACM pair at 597/598 m on the central offshore mooring (Table 2, OC05 and OC04, respectively). The statistics are nearly identical, and the vector correlation had a magnitude of 0.98 and a phase of 6°. The phase difference indicates a bias between this particular pair, with the RCM5 rotated clockwise from the VACM, although the phase difference is within the specification for the compass. Further details of the deployments, current meters, and sampling are given in Appendix A.

The mooring time series were quality-controlled by examining plots of the daily means and variances. A few of the records were truncated early because the daily variances became suspiciously low relative to observations at similar depths on neighboring moorings. (Table 1 record lengths reflect intervals of good data.) Mooring locations were determined by triangulation on the acoustic releases. Instrument depths were determined from measured pressures and wire cuts. Mooring knock down, as determined from the pressure observations, was negligible with the exception of the second deployment of mooring OC. Pressure gauges at all depths on OC recorded an increase in pressure between December 1994 and February 1995 with extreme downward displacement of the instruments through the water column ($\sim$ 90 m) in early January. Pressures were approximately constant for the rest of the record.

The goal of this study is to describe variability below about 0.1 cpd. The time series were low-pass filtered with a fourth-order Chebyshev filter with a cutoff of 40 hours,

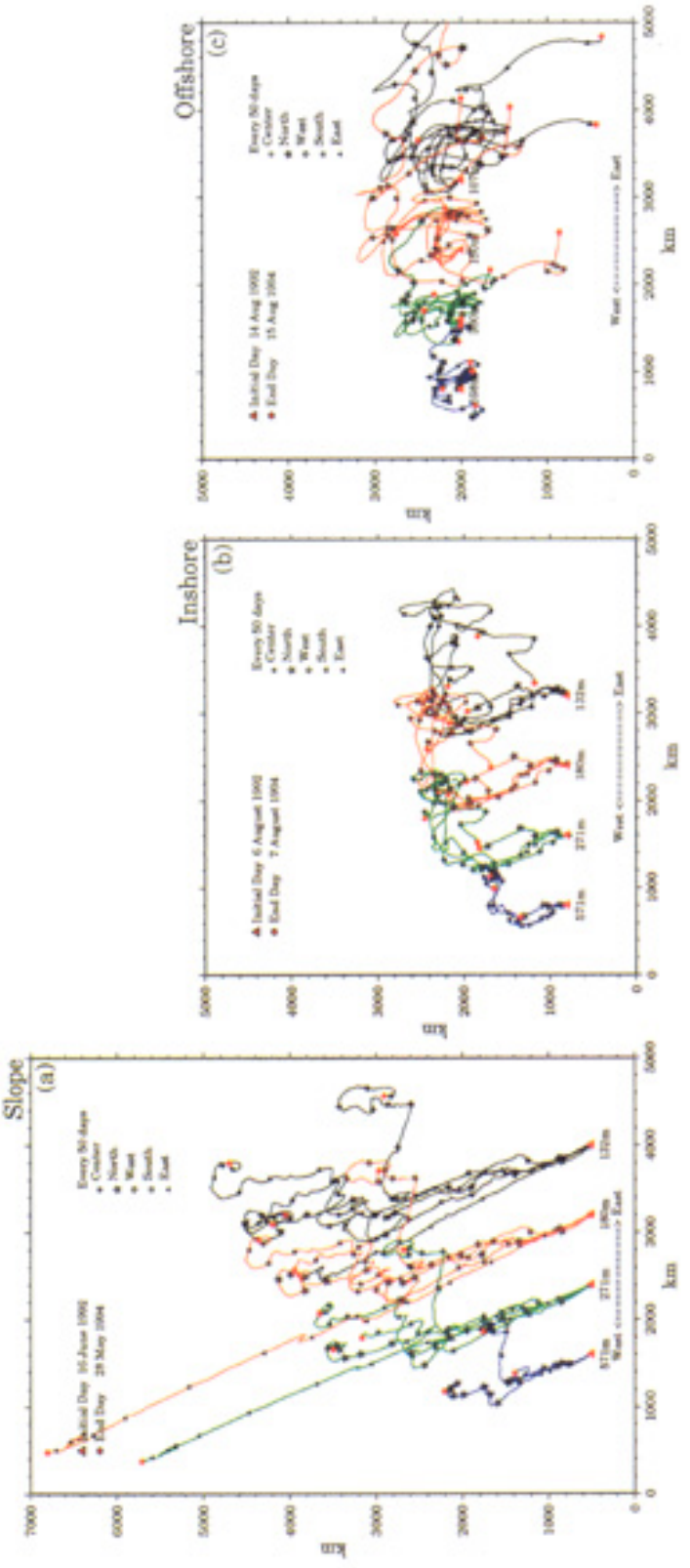

Plate 2. Progressive vector diagrams showing particle displacement due to advection by the low-frequency and mean flows over the 2-year period 1992-1994 at the three local dynamics arrays (LDAs). Displacements were calculated by integrating the low-pass-filtered velocity time series. Depths are color-coded and offset for clarity. Symbols distinguish different moorings, with a symbol plotted every 50 days. The solid red triangles mark the initial day; the solid red circles mark the final days.

Table 1. Mooring Information

Mooring	Latitude, °N	Longitude, °W	Water Depth, m	Instrument Depth, m	Record Dates	Current Meter Type
			Offshore LDA			
OW01	37.053	127.703	4750	106	Aug. 1992 to Aug. 1994	VACM
OW02				156	Aug. 1992 to Aug. 1994	VACM
OW03				305	Aug. 1992 to Dec. 1993	RCM8
OW04				605	Aug. 1992 to April 1994	RCM5
ON01	37.215	127.618	4742	102	Aug. 1992 to Aug. 1994	VACM
ON02				152	Aug. 1992 to Aug. 1994	VACM
ON03				301	Aug. 1992 to Jan. 1994	RCM8
ON04				601	Aug. 1992 to April 1993	RCM5
OE01	37.147	127.410	4663	106	Aug. 1992 to April 1993	VACM
OE02				156	Aug. 1992 to April 1993	VACM
OE03				300	Aug. 1992 to April 1993	RCM8
OE04				600	Aug. 1992 to Oct. 1992	RCM5
OS01	36.982	127.495	4757	106	Aug. 1992 to March 1994	VACM
OS02				156	Aug. 1992 to Aug. 1994	VACM
OS03				305	Aug. 1992 to May 1993	RCM8
OS04				605	Aug. 1992 to Aug. 1994	RCM5
OC01	37.112	127.535	4752	98/50	Aug. 1992 to Aug. 1996	VACM/RCM8
OC02				148/100	Aug. 1992 to Aug. 1996	VACM/RCM8
OC03				298/250	Aug. 1992 to Aug. 1996	VACM/RCM8
OC04				598/550	Aug. 1992 to Aug. 1996	VACM/RCM8
OC05				597	Aug. 1992 to Aug. 1994	RCM5
			Single Mooring			
IOC02	37.820	125.852	4320	150	Aug. 1992 to Aug. 1994	RCM5
IOC03				300	Aug. 1992 to Aug. 1994	RCM5
IOC04				600	Aug. 1992 to Aug. 1994	RCM5
			Inshore LDA			
IW01	38.426	124.358	3619	120	Aug. 1992 to Aug. 1994	VACM
IW02				172	Aug. 1992 to Aug. 1994	VACM
IW03				322	Aug. 1992 to Aug. 1994	VACM
IW04				623	Oct. 1992 to Apr. 1994	VACM
IN01	38.607	124.344	3438	115	Aug. 1992 to Dec. 1993	VACM
IN02				167	Aug. 1992 to Aug. 1994	VACM
IN03				318	Aug. 1992 to Aug. 1994	VACM
IN04				618	Oct. 1992 to Apr. 1994	VACM
IS01	38.414	124.133	3504	132	Aug. 1992 to Aug. 1994	VACM
IS02				185	Aug. 1992 to March 1994	VACM
IS03				335	Aug. 1992 to Aug. 1994	VACM
IS04				633	Oct. 1992 to April 1994	VACM
IC01	38.508	124.238	3408	126	Aug. 1992 to Aug. 1994	VACM
IC02				181	Aug. 1992 to Aug. 1994	VACM
IC03				328	Aug. 1992 to Aug. 1994	VACM
IC04				618	Oct. 1992 to April 1994	VACM

twice the local inertial period. The filter removed the energetic tidal and inertial components. Prior to filtering, the records were linearly interpolated to standard depths, chosen to be the closest depths to the target depths without requiring any extrapolations. Standard depths at the offshore array were 107 m, 150 m, 300 m, and 598 m. Standard depths at the nearshore (inshore and slope) arrays were 132 m, 180 m, 271 m, and 598 m. Records that were formed using two deployments were first interpolated to standard depths, then joined, and low-pass filtered.

The analyses presented in subsequent sections use interpolated, low-pass-filtered data. Generally, interpolated depths are close to the observed depths when the data records are complete. We filled data gaps at 150 m using linear interpolation from the records at 100 and 300 m, because a linear estimate gave a good approximation to the expected signal variance. We did not fill the gaps at 300 m, because there was a significant error (about 50%) in the signal variance based on a linear estimate; we did not try a higher-order interpolation. No extrapolations were used.

Table 1. (continued)

Mooring	Latitude, °N	Longitude, °W	Water Depth, m	Instrument Depth, m	Record Dates	Current Meter Type
			Slope LDA			
MW01	38.596	124.106	2602/2615	89/158	June 1992 to June 1994	RCM8/ADCP
MW02				140/167	June 1992 to June 1994	RCM8
MW03				288/314	June 1992 to June 1994	RCM8
MW04				588/609	June 1992 to June 1994	RCM8
MN01	38.776	124.079	1972/1975	78/132	June 1992 to June 1994	RCM8/ADCP
MN02				128/142	June 1992 to June 1994	RCM8
MN03				276/294	June 1992 to June 1994	RCM8
MN04				574/590	June 1992 to June 1994	RCM8
MS01	38.585	123.909	1975/1975	102/132	June 1992 to June 1994	RCM8/ADCP
MS02				/144	May 1993 to June 1994	RCM8
MS03				302/292	June 1992 to June 1994	RCM8
MS04				/597	May 1992 to June 1994	RCM8
MC01	38.670	123.985	1975/1975	107/115	June 1992 to June 1994	RCM8
MC02				158/124	June 1992 to June 1994	RCM8
MC03				309/272	June 1992 to June 1994	RCM8
MC04				608/572	June 1992 to June 1994	RCM8
ME01	38.744	123.856	415/415	82/	June 1992 to May 1993	RCM8
ME02				133/174	June 1993 to June 1994	RCM8
ME03				285/323	June 1992 to June 1994	RCM8

Moorings designated O, IO, I, and M correspond to offshore, single, inshore, and slope array, respectively. Array code E, W, etc., refers to position within the array. The slope array was redeployed after 1 year. Mooring OC was redeployed after 2 years. LDA, local dynamics array.

3. Time series analysis

3.1. Means

Variability dominates over mean flow at all moorings, with means less than one standard deviation (Table 2). The orientation of the principal variance [*Priesendorfer*, 1988] is north-south at most locations, in particular at the slope LDA, where the alignment closely parallels that of the bathymetry (330°T). At the central mooring of the offshore array (OC), principal variance orientation is meridional during the first 2 years (Table 2) but becomes more isotropic during the second 2-year interval.

The offshore LDA is situated in a regime where geostrophic calculations indicate a mean equatorward flow [*Wyllie*, 1966; *Hickey*, 1979], while the nearshore arrays include the continental slope regime where geostrophic and direct estimates indicate the existence of poleward subsurface flow within the California Undercurrent (CUC) [e.g., *Chelton et al.*, 1988; *Collins et al.*, 1996; *Garfield et al.*, 1999]. In fact, there is little evidence of a mean equatorward California Current at the offshore LDA and single mooring (Table 2). The progressive vector diagrams (PVDs) map the particle displacements due to advection by the low-frequency and mean flows over the 2-year period (Plate 2). There is a small net eastward displacement at the offshore LDA, with no significant meridional displacement. Flow at the offshore LDA is dominated by eddy-like motions, with large rotary excursions evident in the PVDs (Plate 2). Displacements are visibly correlated between moorings and between instrument depths. The flow is surface-intensified, with order of magnitude larger displacements occurring at shallow depths relative to deep ones. Although the mean flow is smaller at the offshore LDA, the vertical shear is larger than that observed at the two nearshore LDAs.

Displacements at the nearshore arrays show persistent flow to the northwest at all depths for the first year of the record. This is the signature of the CUC, extending from the shelf to the westernmost mooring, ~ 100 km offshore. *Chelton et al.* [1988] have previously observed this undercurrent as far offshore as 150 km. Flow is visibly coherent at different moorings and instrument depths (Plate 2). *Kosro et al.* [1994] noted the presence of a concentrated poleward undercurrent over the slope array (subsurface velocity maximum at depths between 150 and 300 m) which decreased in speed with increased distance from the shore. The flow was strongly aligned with the topography even though the water depth exceeds 1900 m at all but one mooring and data are from the upper 600 m of the water column. Inclusion of data from the four moorings of the inshore array located to the west of the slope array extends their results to the deeper water (~ 3500 m) offshore of the continental slope. The direction of flow is very similar at both arrays for the first year although the flow has a slightly more northward component in the deeper water array. The observation that mean flow speeds decrease with distance from shore (compare displacements from IN with MS) is upheld with the inclusion of data from the inshore LDA. In the second year, a change in behavior is evident at the nearshore arrays. At all but the

Table 2. Mooring Statistics

Mooring	$\overline{u}$, cm s^{-1}	$\overline{v}$, cm s^{-1}	$\overline{T}$, °C	$\overline{u'u'}$, cm^2 s^{-2}	$\overline{v'v'}$, cm^2 s^{-2}	$\overline{T'T'}$, °C^2	$\overline{u'v'}$, cm^2 s^{-2}	$\overline{u'T'}$, °C cm s^{-1}	$\overline{v'T'}$, °C cm s^{-1}	θ, °T	τ, days
Offshore LDA											
OW01	4.5	0.2	11.6	70.35	117.43	1.66	-61.49	1.73	0.87	-34.5	27.3
OW02	2.7	0.1	9.6	54.30	117.10	0.61	-46.10	0.70	0.89	-27.9	16.2
OW03	0.7	0.6	7.3	21.79	58.44	0.34	-21.97	-0.33	0.07	-25.1	9.7
OW04	-0.1	1.3	4.9	6.22	8.66	0.04	-3.58	-0.00	0.07	-35.6	13.7
ON01	4.9	-0.7	11.1	71.62	128.42	1.49	-23.36	2.67	1.68	-19.7	14.5
ON02	4.2	0.3	9.1	54.81	104.05	0.53	-20.12	1.73	1.78	-19.6	19.0
ON03	2.7	0.5	7.2	24.65	52.05	0.38	-12.61	1.04	1.44	-21.3	17.0
ON04	1.1	0.1	4.9	9.09	14.32	0.06	-4.00	0.26	0.01	-28.4	20.1
OE01	2.0	2.7	10.6	90.74	150.17	1.90	-39.92	4.22	3.47	-26.7	10.4
OE02	0.6	4.0	9.0	75.69	132.24	0.70	-44.99	-0.58	5.21	-28.9	8.4
OE03	0.2	2.2	7.1	21.08	41.93	0.27	-10.56	-0.49	1.76	-22.7	10.1
OE04	4.3	-2.8	5.1	22.27	14.08	0.06	-15.00	-0.46	0.56	-52.6	6.7
OS01	1.2	-3.1	11.2	101.88	146.88	1.59	-16.83	2.69	2.25	-18.4	12.5
OS02	0.3	-1.7	9.2	82.08	110.68	0.53	-12.24	-0.86	0.39	-20.3	15.2
OS03	-1.2	0.1	7.3	39.39	61.51	0.30	-9.13	-2.22	-0.68	-19.8	10.9
OS04	-0.3	-0.2	5.0	7.71	17.61	0.08	-1.79	-0.31	-0.14	-9.9	12.6
OC01[a]	3.1	-3.1	11.3	77.64	154.32	1.37	-27.40	2.73	2.20	-17.8	7.6
OC02[a]	2.6	-0.8	9.5	75.28	109.71	0.77	-33.54	0.40	1.02	-31.4	11.8
OC03[a]	0.9	-0.5	7.2	20.99	57.37	0.35	-11.78	-0.54	0.00	-16.5	9.7
OC04[a]	0.4	-0.1	4.9	7.34	19.32	0.08	-5.29	0.00	-0.09	-20.7	18.0
OC05[a]	0.4	-0.2	4.9	5.75	16.93	0.08	-3.05	0.01	-0.08	-14.3	13.2
OC01[b]	2.4	-1.9	11.3	64.01	37.97	1.06	0.99	-0.75	-1.21	87.8	8.6
OC02[b]	1.8	-1.8	10.2	47.54	31.69	0.60	5.26	-0.39	-0.79	73.2	10.2
OC03[b]	0.4	-1.2	7.2	20.23	23.20	0.08	7.94	-0.20	-0.35	39.7	15.5
OC04[b]	-0.3	-0.8	5.1	10.56	12.07	0.06	4.55	-0.21	-0.40	40.3	17.7
OC01[c]	2.8	-2.4	11.3	70.42	90.53	1.20	-11.96	0.82	0.31	-25.0	7.0
OC02[c]	2.2	-1.3	9.8	61.59	71.16	0.81	-14.00	-0.11	-0.06	-35.6	13.0
OC03[c]	0.6	-0.8	7.2	20.78	40.52	0.21	-1.89	-0.37	-0.16	-5.4	13.0
OC04[c]	0.1	-0.5	5.2	9.85	18.22	0.09	-0.69	-0.08	-0.22	-4.7	14.7
Single Mooring											
IOC02	1.1	0.9	8.7	46.48	28.99	0.20	2.88	0.90	-0.42	80.9	7.6
IOC03	0.0	0.9	7.0	22.43	13.93	0.13	1.77	0.26	-0.02	78.7	9.4
IOC04	-0.1	0.8	5.0	12.35	7.18	0.04	-0.45	0.14	0.02	-85.1	11.3

shallowest mooring, alternating flow directions are evident in the particle displacements (Plate 2).

Our findings confirm those of *Stabeno and Smith* [1987], who also observed small-amplitude mean but large-amplitude eddy-like flows in the currents above 600 m. However, unlike the records available to *Stabeno and Smith* [1987], our current records are highly correlated between adjacent moorings and depths, resolving eddy events across the arrays. It is this mesoscale variability that is the focus of the remainder of this paper.

3.2. Variability

Velocity records within arrays are visually correlated both horizontally and vertically. Plate 3 shows time series of daily averaged velocity and temperature from mooring pairs within each LDA and the full 4-year record at mooring OC. At each array, the vectors generally fluctuate together, showing high vertical coherence and a decay in amplitude with depth. There are, however, several striking examples in the time series when the currents at moorings separated by only 15 km apparently flow in opposite directions over periods of days to weeks. Two such periods at the offshore array are May and November-December 1993 (Plate 3a). These events correspond to the passage of eddies directly over the array, described below and in greater detail in section 5.

At the offshore array, little net displacement of water was seen in the progressive vector plots (Plate 2). This is confirmed by the vector time series which show a preferred orientation (N-S) but not a preferred current direction. Instead, rather slow variations are seen with flow alternating north and south. There are three time periods over the 4-year deployment during which velocities are larger than typical background levels. These intensified flow events have been marked by vertical lines in Plate 3. The first event is in April-May 1993, the second occurs in November-December 1993, and the third event, for which there is only one mooring, occurs around January 1995.

Prior to the first event, there is a slow turning of the current to the north at all depths, with records from both moor-

Table 2. (continued)

Mooring	$\overline{u}$, cm s^{-1}	$\overline{v}$, cm s^{-1}	$\overline{T}$, °C	$\overline{u'u'}$, cm^2 s^{-2}	$\overline{v'v'}$, cm^2 s^{-2}	$\overline{T'T'}$, °C^2	$\overline{u'v'}$, cm^2 s^{-2}	$\overline{u'T'}$, °C cm s^{-1}	$\overline{v'T'}$, °C cm s^{-1}	θ, °T	τ, days
					Inshore LDA						
IW01	0.2	0.6	8.7	71.62	118.02	0.17	14.67	0.29	-0.83	16.2	8.1
IW02	-0.0	1.4	8.1	61.21	97.83	0.15	8.63	0.29	-0.39	12.6	8.2
IW03	-0.1	1.7	7.2	40.30	64.17	0.12	3.57	0.25	0.06	8.3	8.9
IW04	-1.2	3.3	5.2	10.70	26.19	0.02	1.26	-0.05	0.08	4.6	4.4
IN01	1.9	2.3	8.6	57.41	71.12	0.13	5.97	0.25	-0.37	20.5	6.6
IN02	1.3	0.5	8.1	57.15	94.76	0.12	-0.46	0.79	-0.42	-0.7	4.7
IN03	1.1	1.0	7.2	37.72	62.07	0.09	-0.90	0.50	-0.05	-2.1	4.9
IN04	0.7	1.0	5.2	12.18	20.35	0.04	-1.40	0.13	0.05	-9.4	6.6
IS01	0.2	2.2	8.7	54.58	66.51	0.19	-12.89	-0.14	0.06	-32.6	6.4
IS02	0.3	2.6	8.2	60.54	67.02	0.15	-13.97	-0.19	0.03	-38.5	6.8
IS03	0.3	2.7	7.3	44.29	47.53	0.12	-9.37	0.01	-0.06	-40.1	6.5
IS04	0.3	1.6	5.3	13.60	10.63	0.04	-2.47	0.01	-0.01	-60.5	6.7
IC01	1.1	1.7	8.7	67.05	117.15	0.17	-6.00	0.47	-0.29	-6.7	5.3
IC02	0.8	2.2	8.2	57.47	87.22	0.15	-6.99	0.43	0.14	-12.6	5.4
IC03	0.7	2.2	7.3	39.72	56.40	0.11	-4.29	0.45	0.27	-13.6	6.0
IC04	0.5	1.4	5.3	9.87	13.31	0.03	-1.26	0.11	0.13	-18.0	6.9
					Slope LDA						
MW01	0.8	4.0	8.7	67.70	85.63	0.20	-24.85	-0.22	1.08	-35.1	7.2
MW02	0.8	4.1	8.2	53.79	62.02	0.15	-18.96	0.11	0.53	-38.9	7.8
MW03	0.6	3.6	7.3	37.55	36.82	0.10	-12.80	0.34	0.10	-45.8	8.6
MW04	0.4	2.1	5.2	13.49	15.88	0.03	-7.27	0.20	-0.05	-40.3	9.9
MN01	-1.3	5.8	8.7	64.71	100.16	0.30	-16.60	-0.42	0.87	-21.6	4.5
MN02	-1.1	5.6	8.2	43.95	64.96	0.20	-14.34	-0.13	0.35	-26.9	5.6
MN03	-1.2	4.9	7.3	28.58	38.63	0.10	-14.87	0.24	-0.10	-35.7	9.1
MN04	-0.7	2.8	5.2	14.27	24.20	0.02	-11.72	0.05	0.03	-33.5	12.7
MS01	-1.5	6.0	9.0	76.90	123.55	0.38	-42.43	-0.23	1.13	-30.6	5.3
MS02	-0.9	5.6	8.5	54.49	95.35	0.28	-36.04	-0.21	0.43	-30.2	5.9
MS03	-1.0	4.5	7.5	29.59	63.30	0.13	-25.82	0.21	-0.62	-28.4	7.1
MS04	0.5	0.7	5.2	13.55	37.16	0.04	-15.55	0.28	-0.48	-26.4	10.2
MC01	-0.3	6.8	8.8	64.39	91.18	0.26	-29.53	-0.02	0.81	-32.8	5.8
MC02	-0.5	6.3	8.3	50.20	68.98	0.18	-26.52	0.19	0.23	-35.2	6.6
MC03	-0.5	5.1	7.4	31.99	45.42	0.11	-22.99	0.38	-0.36	-36.9	9.8
MC04	-0.6	2.5	5.2	7.47	18.19	0.03	-7.90	0.04	-0.01	-27.9	7.2
ME01	-5.4	11.7	9.0	56.89	116.77	0.45	-61.48	0.71	-0.86	-32.0	4.2
ME02	-4.4	10.2	8.4	37.06	110.23	0.25	-53.57	0.49	-1.00	-27.8	11.6
ME03	-3.3	8.4	7.6	18.07	88.81	0.10	-36.98	0.34	-0.86	-23.1	16.5

Record length means, variances, and covariances of low-pass-filtered east velocity u, north velocity v, and temperature T, the major axis orientation of the velocity principal variance θ [*Priesendorfer*, 1988], and the integral timescale τ [*Davis*, 1976; *Stabeno and Smith*, 1987]. Depths for the offshore and single mooring: 1=107 m, 2=150 m, 3=300 m, and 4=598 m. Depths for the inshore and slope array: 1=132 m, 2=180 m, 3=271 m, and 4=571 m.

[a]First deployment statistics, 1992-1994. OC05 statistics were calculated from the low-pass-filtered RCM5 series at 597 m for comparison with OC04, the VACM series at 598 m.

[b]Second deployment statistics, 1994-1996.

[c]Combined statistics, 1992-1996.

ings following each other closely. During the event, opposing currents that last for about a week are observed across the array. Flow at the northernmost mooring (ON) is northward, while southward currents are seen at the central mooring (OC), only 15 km away (Plate 3a). Horizontal velocity gradients at the array center were estimated by a least squares function fit (a plane) to the observations at a given depth level (see Appendix B). We assumed a residual variance that was about 20% of the expected signal variance. Horizontal divergence ($D = u_x + v_y$) calculated over the array is not significantly different from zero (Figure 1a). The relative vorticity ($\zeta = v_x - u_y$) is large and negative during the May eddy (Figure 1a), consistent with clockwise rotation of currents. A southward current persists after the event at both moorings. A similar pattern is evident for the second event in November although the buildup of northward flow prior to the event is more rapid and the southward flow after the event is stronger and more persistent. The third event (January 1995) is characterized by a rapid transition from weak southeastward to strong southwestward flow (Plate 3b). The events are associated with increases in daily averaged temperature (shown above velocity vec-

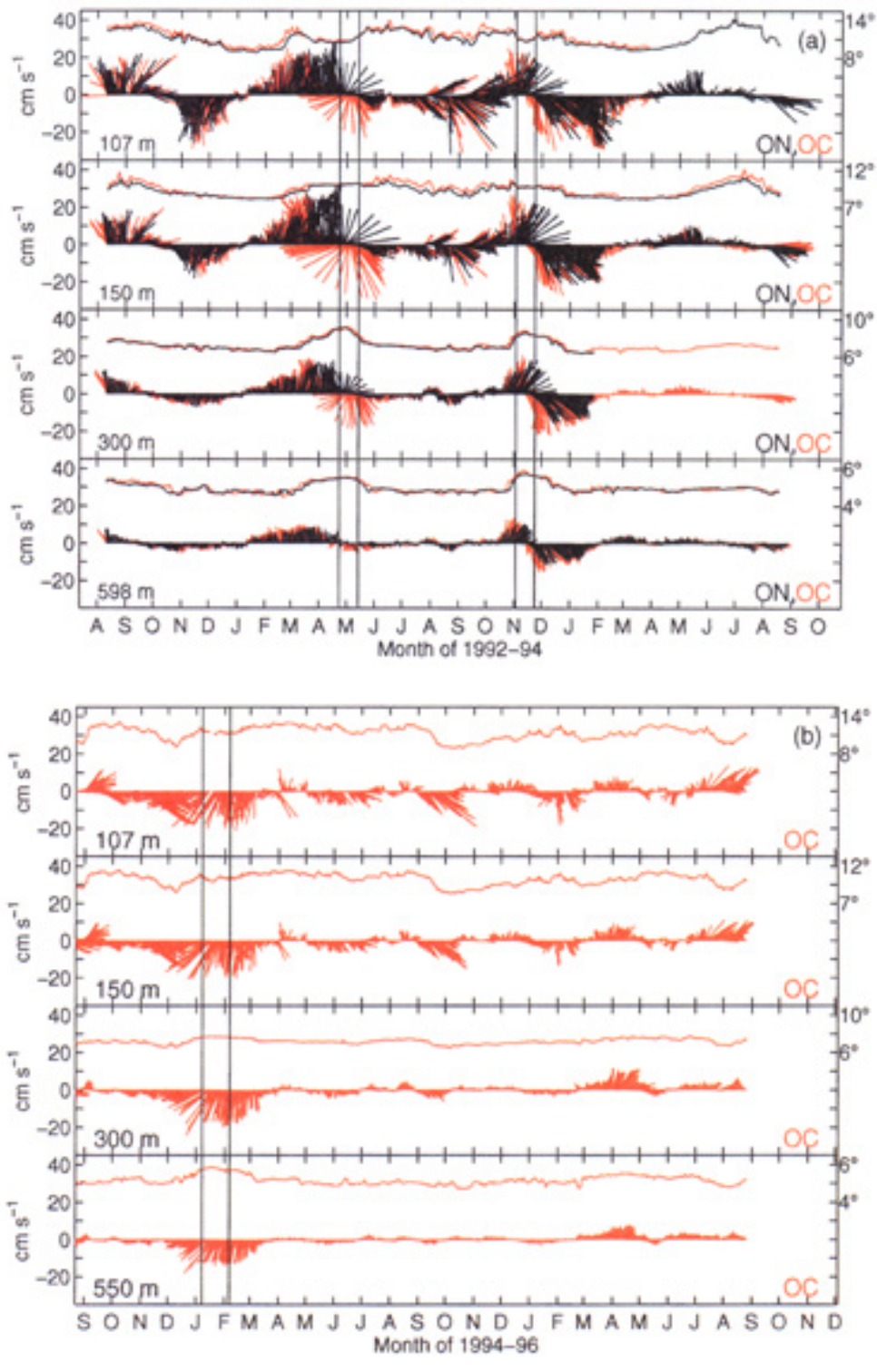

Plate 3. Daily averaged velocity vector and temperature time series for two moorings at each array. Individual moorings are distinguished by color. Event time periods are indicated by vertical lines. (a) Offshore array, first 2-year deployment. ON (black) is compared to OC (red). (b) Offshore array OC, second 2-year deployment. (c) Slope array. MS (black) is compared to MN (red). (d) Inshore array. IS (black) is compared to IC (red).

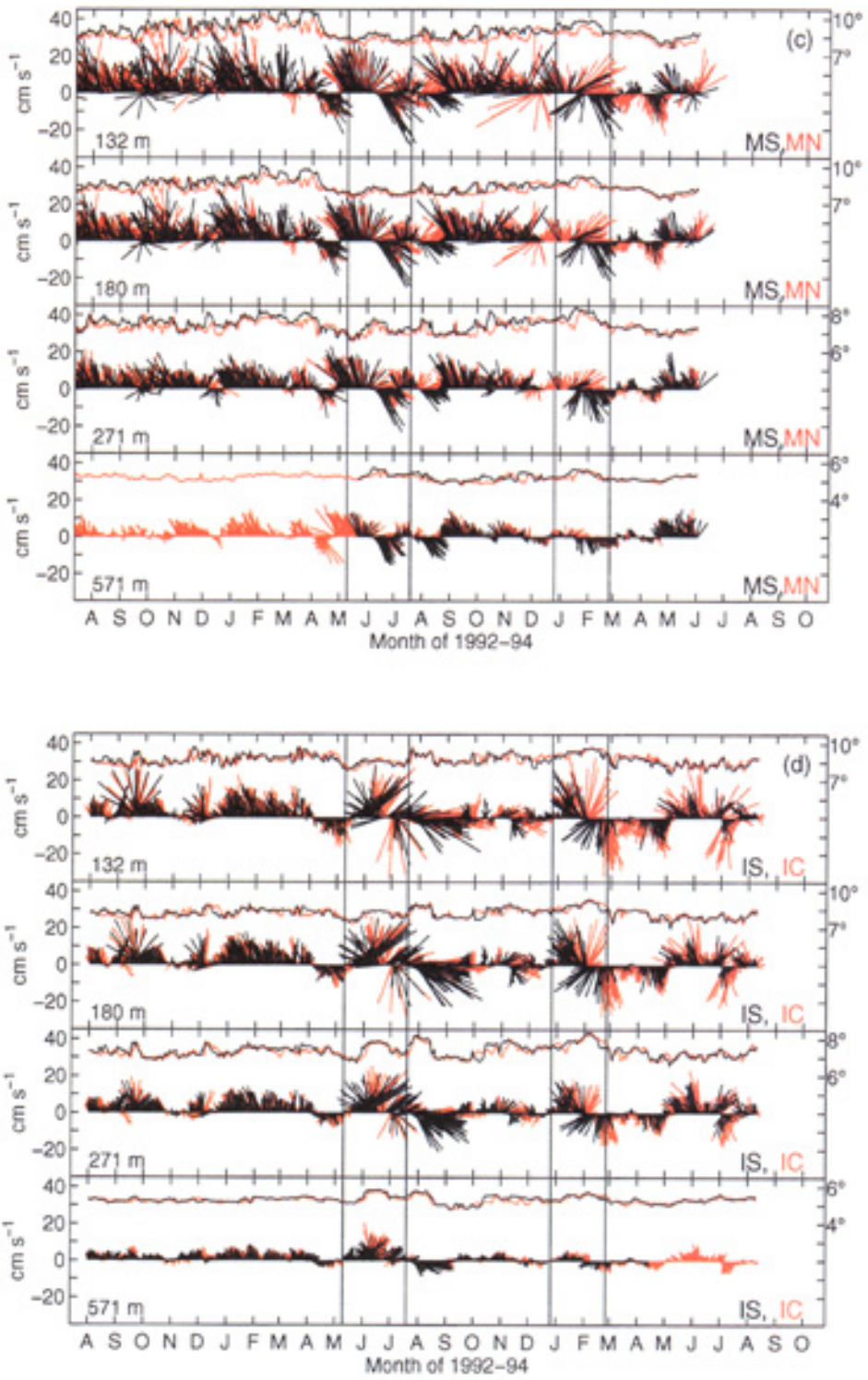

Plate 3. (continued)

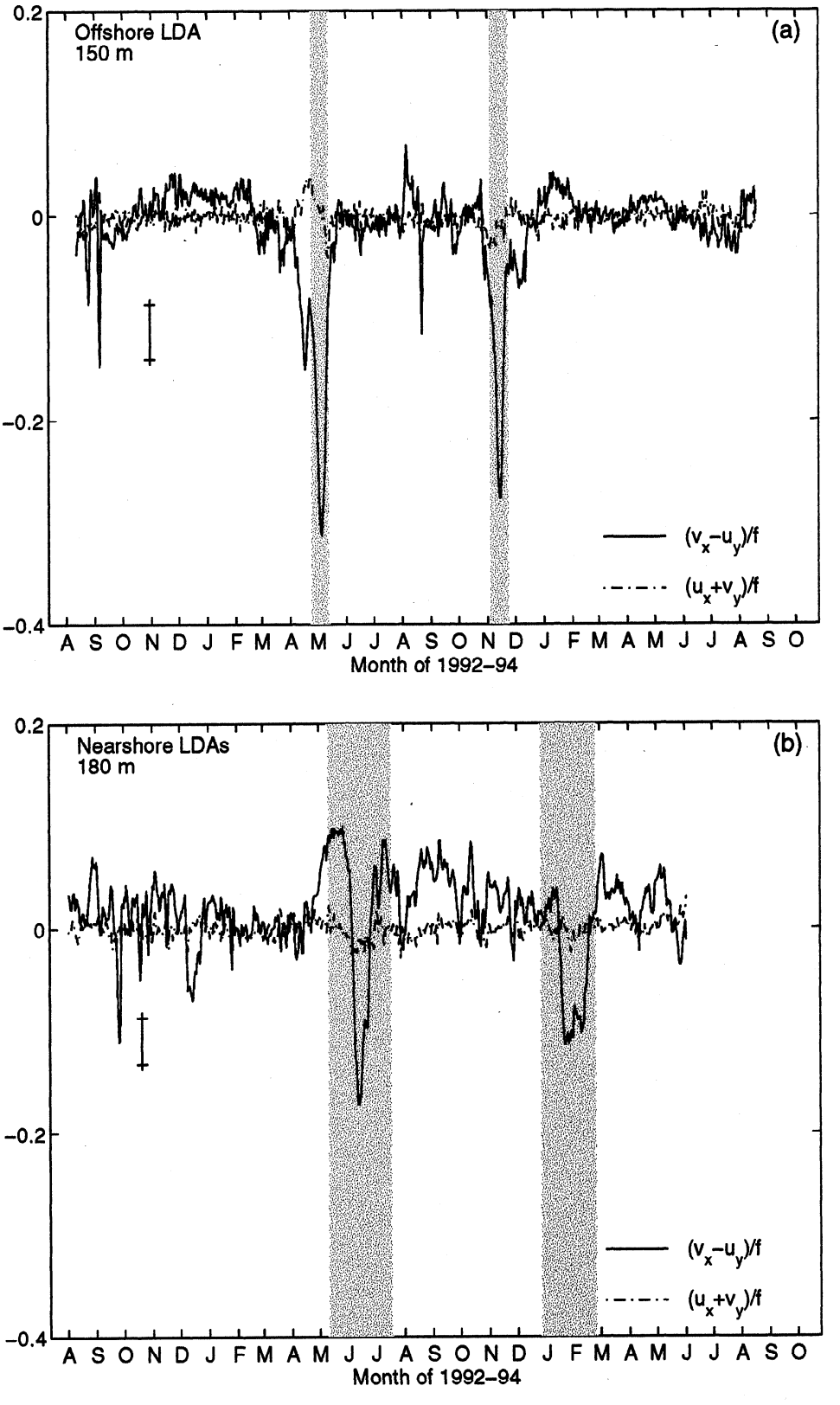

Figure 1. Horizontal divergence D (dashed-dotted line) and relative voticity ζ (solid line) normalized by local planetary vorticity f. Shaded intervals correspond to event time periods marked in Plate 3. The error bar shown is based on complete data (all moorings present). (a) Estimates made for the offshore LDA at depth 150 m. (b) Estimates made for the combined nearshore LDAs at depth 180 m.

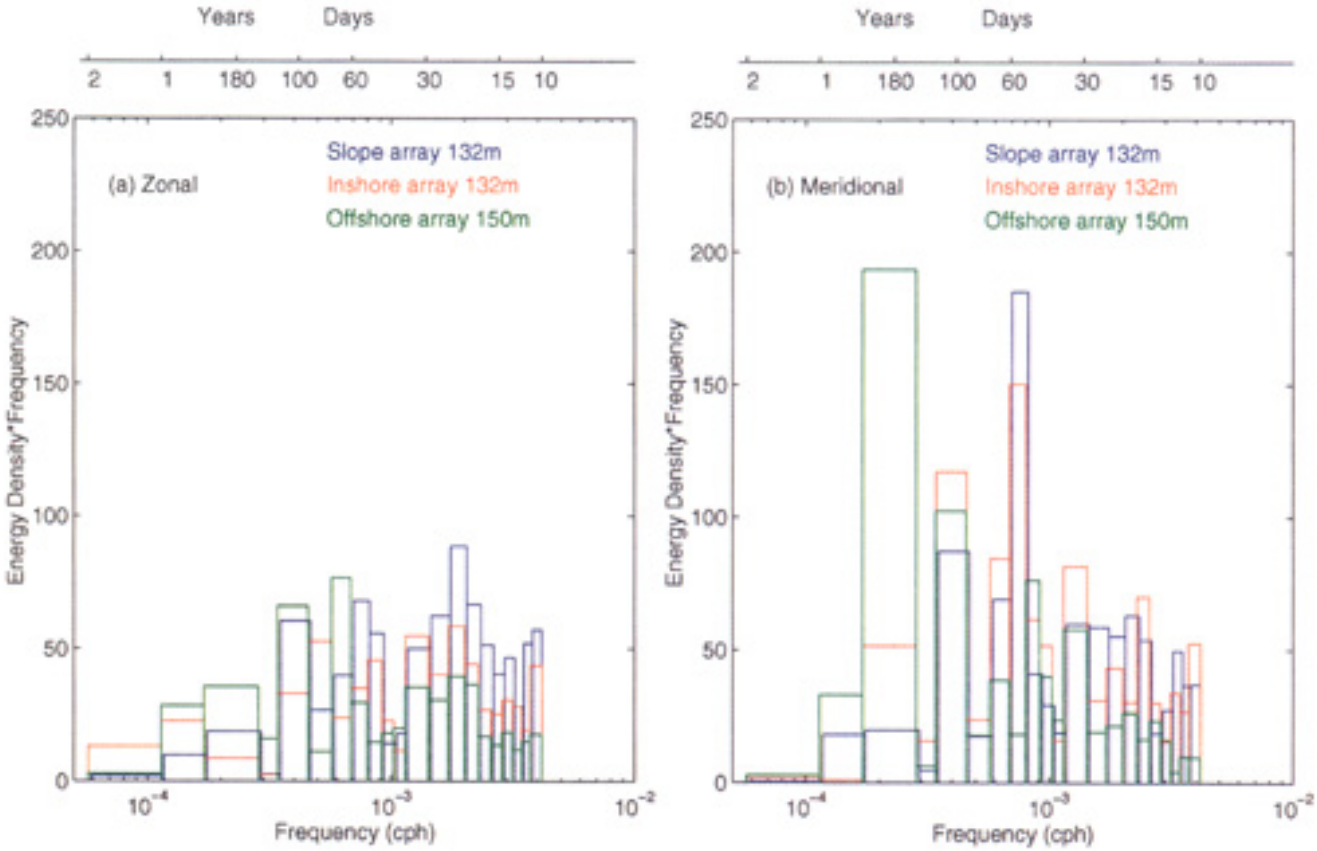

Plate 4. Velocity spectra plotted in variance-preserving form for 2-year deployment beginning summer 1992. Individual spectra have been averaged over arrays; arrays are distinguished by color: (a) zonal velocity ($cm^2\ s^{-2}$) and (b) meridional velocity ($cm^2\ s^{-2}$).

tors) at the two lower levels (Plates 3a and 3b). In section 5, we argue that these events are signatures of deep warm core eddies that have formed close to the coast and propagated westward across the offshore array, similar to anticyclones observed by *Huyer et al.* [1998] during SeaSoar surveys which were made during June and August 1993 from approximately 36°N to 39°N and from the continental slope to 128°W.

Rapid fluctuations and transitions in alongshore current are seen over the continental slope (see MS/MN, Plate 3c). Indeed, the most striking geographical difference between the nearshore and offshore arrays lies in the frequency and the duration of eddy events. Over the 4-year record at OC, there are 3-5 eddy events that stand out visually in the time series, and the duration of each of these events is 90-120 days. Roughly double that number of events occur over the 2-year record measured at the slope array, and the dominant timescale is about 60 days. At the inshore site (IS/IC, Plate 3d), there is an increased tendency for rotary variations rather than alongshore current pulsing. There are no reversals of flow direction over the first year as a result of the strong mean poleward flow. Eddy-like fluctuations are especially evident in the second year of deployment. There are several instances when the velocity field appears to diverge over the arrays but is actually horizontally nondivergent because u_x balances v_y (Figure 1b). We assumed a larger error variance (30% of expected signal variance) for the combined arrays to account for more model error in fitting a plane over two arrays. Relative vorticity of both signs is apparent in the 2-year time series, but the largest-amplitude and longest-duration events appear to be anticyclones (Figure 1b). These events will be examined in greater detail in section 5, where we show that the patterns during these events are consistent with the presence of an eddy spanning the two nearshore LDAs. Variability during these events displays similar eddy-like characteristics to those discussed at the offshore array. The eddy velocity signal extends to the deepest sampled levels, and daily averaged temperatures indicate a warming of the deeper water column (see records at 271 m and 571 m, Plates 3c and 3d).

3.3. Spectra

We use velocity spectra to examine the distribution of velocity variance as a function of frequency and to illustrate the shift to lower frequency of the dominant energy band with distance offshore. Because we wanted to retain the lowest frequency resolved by the record, the spectra were computed from the full time series, with no piecewise averaging. Spectral estimates were then averaged in variable length frequency bands for clarity and to increase statistical confidence at higher frequencies; little or no averaging over low-frequency bands was performed. The spectra are useful in displaying the frequency distribution of energy for this 2-year time period, regardless of how representative they may

be of a longer time period. We use the 4-year series at OC and the 2-year series at the mid–California Current location to address the issue of representativeness.

The orientation of the principal variance was generally meridional (Table 2) during the 2-year period, although it varied substantially between moorings. For this reason we chose to compute spectra for the northward (v) and eastward (u) components rather than rotate into a principal variance frame (Plate 4). The spectra from each LDA were averaged (there were four sufficiently long records at the slope and offshore LDA but only three at the inshore LDA). The shelf mooring (ME) was not included in the spatial average for the slope array, as the spectra were quite distinct from the other deep water moorings in the array. The level closest to 150 m is chosen for display purposes; other levels show similar distributions.

Energy levels were higher for north-south velocities, which follows from the principal variance orientation and from prior comments that flow is closely aligned to topography (running approximately in the north-south direction). There is a pronounced energy peak at the 60-day band for the two inshore arrays (Plate 4). By contrast, the highest peak at the offshore site is at a much lower frequency range centered at period $T \sim 180$ days. Although there is no sharp peak at 60 days at the offshore site, spectra at all three arrays show a general increase in energy in a band between 40 and 70 days as well as 90 and 120 days. Energy levels in the 40- to 70-day band are reduced at the offshore array compared to the inshore spectra. The situation is reversed at low frequencies ($T > 140$ days). Clearly, this is the dominant band for the offshore array which is not well resolved with the 2-year time series. All arrays show a reduction of northward kinetic energy at high frequencies (periods less than ~ 40 days) as well as midrange frequency minima at periods of ~ 80 and ~ 140 days.

We use the 4-year record at the central offshore mooring to examine the representativeness of the 2-year records. Because the principal variance was more isotropic during the second deployment, we show the distribution of kinetic energy rather than the individual components (Figure 2). As before, spectral estimates from the 4-year series were computed with little or no averaging at the lowest frequencies; a band-averaged estimate with increased statistical confidence is overlaid for comparison. The estimates from the separate first and second 2-year deployments averaged over the same frequency bands are also shown. Confidence limits at 95% significance based on the 1992-1996 spectral estimates (our best guess at the true spectra) are overlaid on the 2-year spectral estimates.

As expected, the band-averaged estimate for the 4-year series usually falls somewhere in between estimates from the first and second deployments. There is more total variance in the first 2-year record than in the second, and these increased energy levels are evident in the OC time series (Plate 3) as well as the spectra. Kinetic energy is enhanced between 180 days to a year and the 40- to 120-day band. Notice that the frequency band averaging blurs out a very distinct peak at 100 days. This was not apparent in the 2-year estimates of Plate 4, as frequency resolution was coarser so that the peak was averaged with the adjacent lower kinetic energy band. A longer time series is required to determine whether the 100-day peak is robust.

The mooring at the mid–California Current site (IOC) had a more nearly zonal orientation of principal variance (Table

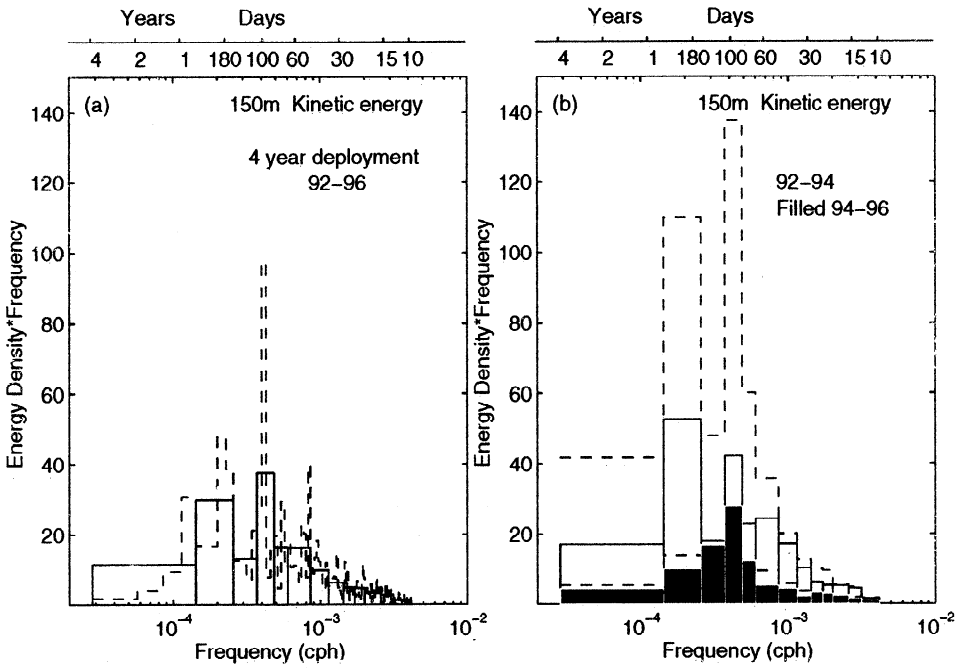

Figure 2. Kinetic energy spectra plotted in variance-preserving form for 4-year deployment at the central offshore mooring OC. (a) Kinetic energy (cm^2 s^{-2}) for 1992-1996 (dashed line). Spectral estimates averaged in frequency bands are shown by the solid line. (b) Kinetic energy (cm^2 s^{-2}) for separate 2-year deployments: 1992-1994 (solid line) and 1994-1996 (solid bars). Estimates have been averaged over frequency bands. Confidence limits at 95% significance level (dashed line) were computed for the averaged 4-year spectrum shown in Figure 2a.

2) and appeared to have lower energy than observed during the same period at the offshore array. There were no obvious eddy events in the record, although at least one eddy was observed to pass directly over the mooring during the June SeaSoar survey [*Shearman et al.*, 1999]. That eddy was a shallow cold cyclone with almost no velocity signature below 150 m, the shallowest measurement depth at IOC. Energy levels at IOC are comparable to the second deployment of OC, excluding the large-amplitude event that occurred in January 1995 (Figure 3), and to the 4-year time series at OC with the three large-amplitude eddy events removed. This background level of variability at both IOC and OC had a magnitude about a third of the identified eddy velocities. Because wind curl forced motions throughout the water column have been observed in the North Pacific north and east of our mooring site [*Niiler et al.*, 1993], we were interested to find whether such directly driven motions were also observable at the OC location over the 4-year time interval. We computed the wind stress curl from NCAR/NCEP reanalyzed surface data in the area surrounding the mooring and its coherence with currents at OC as a function of frequency. While significant coherences at the 95% confidence interval were computed for currents oriented at 45°T, the period of the significant coherent band, the spatial distribution of the coherence around the mooring site, and its amplitude depended upon the length of the record. The 3-year record gave a very different picture than the full 4-year record, and we abandoned the search for directly wind driven currents at this site. These inconclusive results are consistent with those of *Rienecker et al.* [1988], who examined the coherence between currents and wind for the current meter observations of *Stabeno and Smith* [1987]. *Rienecker et al.* [1988] found significant coherence (95% confidence) over a 2-year interval in some frequency bands; however, less than half of the upper ocean current variance (depths of 150 m and 350 m) was explained by the large-scale wind field, leading them to conclude that other effects such as small-scale local wind forcing were also important sources for the observed variability. The nature and the source of the energetic variations in the records when the eddies were not present remains a topic of further investigation.

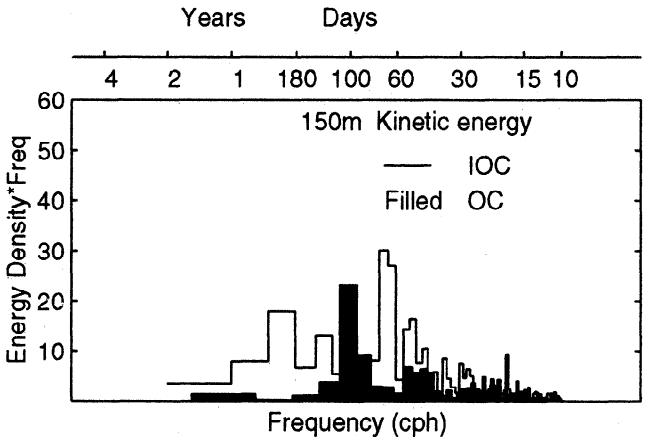

Figure 3. Comparisons of background kinetic energy (no eddy events apparent in time series) at the central offshore (OC) and mid-California Current (IOC) sites. The period analyzed at OC is from March 1995 until August 1996. The period analyzed at IOC is from August 1992 until August 1994.

To summarize, a shift to lower frequencies is evident between the nearshore arrays and the offshore array spectra. The dominant band of variability corresponded to a period of about 60 days for the nearshore arrays, shifting to about 180 days at the offshore array. We hypothesize that many eddies are generated in the highly variable coastal transition zone, so that the dominant band at the nearshore sites has a relatively short period centered around 60 days. Once generated, some eddies propagate westward past our offshore array, while others may dissipate or miss the array. Eddies do not appear to fill the CCS in a dense, compact form from the coast to 128°W; there appear to be large spaces between them as one moves offshore. At least one eddy reaching the offshore site is likely to have originated near the continental margin [*Cornuelle et al.*, this issue] on the basis of its water properties. Similarly, the SeaSoar surveys identified an offshore eddy that could be traced by properties to an origin near the coast [*Huyer et al.*, 1998]. The eddy kinetic energy calculated from surface drifter climatology drops markedly as one moves offshore (Plate 1), suggesting that the eddy energy is removed from the surface layer, either by dissipation or some vertical transfer mechanism. *Kelly et al.* [1998] used moored current observations at the offshore array together with drifters deployed during EBC and Topex altimetry to examine the temporal and geographic distribution of eddy kinetic energy. They found that the monthly maximum in eddy kinetic energy migrated westward to about 128°W on a seasonal timescale, with maximum values in summer-fall. We find that the eddy kinetic energies computed from longer time series including the nearshore arrays support their results, although our spatial coverage is limited to three longitudes (124°W, 126°W, and 128°W). Interestingly, the geographic cutoff that they observed at 128°W from altimetric estimates [see also *Strub and James*, 1999] corresponds to the 500- to 700-km-wide band of enhanced variability apparent in the drifter climatology (Plate 1). A similar drop in variance is also seen in upper ocean temperature, calculated from expendable bathythermograph (XBT) climatology (W. White, personal communication, 1998). However, the altimeter has the best spatial coverage of the three large-scale data sets (XBT, drifters, and Topex). The mechanism by which the eddy energy is removed from the surface layer, apparently on seasonal timescales, is an interesting question, although beyond the scope of this study.

4. Patterns of Variability

Flow variability measured at each current meter includes large-scale fluctuations that are correlated across the array as well as small-scale variations that are not resolved by the horizontal and vertical instrument spacings. Empirical orthogonal functions (EOFs) provide a means of extracting variability that is coherent across the arrays; a truncated sum

of EOFs acts as a filter and is the most efficient estimator of resolved velocity variance [*Davis*, 1976].

We computed velocity EOFs by forming velocity moment matrices for the individual arrays and for the combined nearshore arrays, treating the east and north components of velocity as scalars. For this computation, means were not removed (hence moment rather than covariance matrix); part of what we wanted the EOF to determine was the mean vertical structure (shear) that was coherent across the arrays. Therefore all four depths at all moorings within an array(s) were combined in a single matrix. The EOF decomposition [*Lorenz*, 1956] requires finding the eigenvalues and eigenvectors of the moment matrix. The orthonormal eigenvectors are a complete set of basis functions and represent the uncorrelated spatial modes of variability. The ratio of each eigenvalue to the total variance is the fraction of variance explained by that mode. For complete data, the time-varying amplitudes or temporal EOFs are the projection of the data on the spatial modes. For data gaps, which in our case results from missing moorings or truncated time series, we solved an inverse problem, finding a least squares estimate of the amplitude. Very short time series were excluded from the analysis.

The first three modes accounted for $50-60\%$, $20-30\%$, and about 10%, respectively, of the total variance. The spatial and temporal EOFs and the percent variance explained by individual modes are presented for the offshore (Plates 5a-5d), inshore (Plates 5e-5h), and combined nearshore arrays (Plates 5i-5l). For our purpose of analyzing eddy events, we will use the offshore and combined nearshore EOF representations in section 5.

4.1. EOFs at the Offshore Array

The first EOF at the offshore array (Plates 5a and 5b) shows that the main mode of variability for this 2-year period is a pulsation of flow aligned with the mean California Current (north-south). Approximately half the data variance is explained by the first mode. Given that variability is usually coherent across each array, a unidirectional first mode implies that the spatial pattern of the second EOF would be cross-shore flow or eddy flow, as it must be orthogonal to the first EOF. Even at this distance offshore, the second mode has largest fluctuations aligned perpendicular to the shore (Plate 5c). The third mode is an array-scale eddy (Plate 5d). The first three modes show little change in direction through the upper 600 m of the water column, and flow speed decreases with depth. Interestingly and probably fortuitously, the pattern of spatial variability as described by the EOFs at the offshore site is very similar to that seen at the inshore site, despite the fact that the coastline and significant topography (which obviously play a role in steering the flow at the inshore site) are hundreds of kilometers away.

The slowly varying flows that characterize the offshore time series display several abrupt changes in flow patterns. Two abrupt transitions in the first and third EOF temporal amplitudes occur in April-May 1993 and November-December 1993 and are indicated by vertical lines (Plate 5a). These are the same intervals that were highlighted in the time series in Plate 3 and Figure 1. The events are characterized by a rapid reversal of direction to the south (EOF 1) and strong anticyclonic rotation (EOF 3). Sudden transitions are not apparent in the cross-shore mode.

4.2. EOFs at the Nearshore Arrays

The spatial structure of the first 3 EOFs of the inshore array (Plates 5e-5h) is very similar to that of the offshore array and the slope array (not shown). The most pronounced difference between the nearshore and offshore arrays is found in the temporal EOF variability. At the nearshore arrays, the first mode amplitude is dominated by the low-frequency pulsation of the poleward flowing undercurrent (Plates 5e and 5i). The alignment at the slope array closely parallels the bathymetry, oriented at 330°T (Plate 5j). The orientation of the pulsations is north-south at the inshore array (Plate 5f) and less aligned with the bathymetry than at the slope array (Plate 5j). The second inshore mode shows sustained strong onshore flow during summer 1993 and otherwise high-frequency variability (Plates 5e and 5g) . The eddy-like mode 3 shows strong anticyclonic rotation during two intervals, which are indicated by vertical lines (Plate 5e and Plate 3). During these two intervals, the poleward undercurrent strengthens (see EOF 1).

It is of interest to examine the connection between variability at the inshore and slope arrays. Even though they are located side by side, there is good reason to suspect that they may be sampling different dynamical regimes. The slope array is centered over the continental slope and thus may experience more high-frequency fluctuations in the form of spin-off eddies from the poleward undercurrent or coastally trapped waves than at the deep water site. One might postulate a connection between the two sites during upwelling season. For instance, equatorward flow over the slope might be accompanied by onshore movement at the deeper water array. The variance that is coherent over the two inshore arrays is examined by computing EOFs of the variance matrix made from velocity data at both arrays (Plates 5i-5l). The dominant mode of combined variability is a pulsation of the poleward flowing undercurrent as for the individual array EOFs. There is a clear reduction in the strength of the fluctuations offshore of the continental slope. Coherence of the first mode is degraded by combining all velocity data, as a smaller fraction of the total variance is explained (40%, Plate 5j) when compared to the the first EOFs of the individual LDAs ($50-60\%$, Plates 5b and 5f). Separation of the energy accounted for by each of the first three EOFs has become more blurred. For the individual EOFs in Plates 5a-5h, there was a marked reduction in variance explained between the first mode and the second and third modes. Now the second and third modes each account for approximately half the variance of the dominant EOF. The second EOF picks out flow with some rotational component with abrupt transitions in amplitude. A strong anticyclonic circulation encompassing both arrays is evident in summer 1993 and early 1994 (see EOF 2). The third EOF shows cross-shore variability with particularly strong onshore flow in summer 1993.

In the next section, we focus on those specific parts of the record corresponding to large-amplitude mesoscale events. At the offshore array, the intervals were picked to coincide with the strong signals in the first and third EOF amplitudes. As we have discussed, these time intervals are associated with rapid transitions of the alongshore flow as well as small velocity divergence and negative relative vorticity. We present evidence to support the hypothesis that these signals are due to eddies that propagate across the offshore array. Inshore variability during two periods that display similar variability characteristics to the offshore events will also be discussed.

5. Close-up Look at Mesoscale Events

5.1. Offshore Events

The evolution of velocity and temperature at the offshore array is used to examine the passage of eddies during two time periods of interest (Plate 6). Daily averaged temperature and velocity at each standard depth were objectively mapped over a rectangular area bounded by the outermost moorings of the offshore array using a Gaussian e-folding scale of 15 km. Noise was chosen to be very small at the moorings so that the estimate closely matches the data there. Mapped velocity vectors at 107 m are overlaid on a vertical average of temperature over the three deepest moorings (150 - 598 m). Vertically averaged temperature is meant to approximate dynamic height at 150 m, although we will show that salinity variations are important in determining density during the eddy events.

Several points are illustrated. First, flow direction is consistent with geostrophy, as inferred from temperature. During the May and November time periods, pulses of negative vorticity with peak amplitudes of $0.3f$ were observed; horizontal divergence was not significantly different from zero ($\pm 0.05f$) and is more sensitive to the gradient calculation, since it is a small residual of terms of opposing signs (Figure 1a). During these same time periods, both sets of panels clearly show westward propagating warm-core eddies (Plate 6). The first eddy (May) propagates in from the northeast and continues moving over the array in a southwestward direction, leaving southward flow in its wake. The second eddy (November) appears to propagate zonally through the array. While the eddies are directly over the array, the temperature at 107 m is cooler than usual (Plate 3), although the vertical integral of temperature is warmer (Plate 6) because of anomalously warmer water at 300 and 600 m (Plate 3). The data are consistent with a warm-core eddy centered below 200 m producing an upward doming of the temperature field above the velocity maximum and downward doming below the center (hence the warmer value for the vertically integrated temperature).

Fortuitously, the May eddy was observed by a hydrographic survey [*Musgrave and Royer*, 1994] which sampled past the offshore array, located between stations 14 and 15, on May 19, 1993 (Figure 4). At the time of the survey, the eddy had propagated about 50 km west of the array, and two conductivity-temperature-depth (CTD) casts were made within the eddy (casts 15 and 16). The size of the eddy was about 80-100 km, as determined from shipboard ADCP measurements with 2-km resolution [*Cornuelle et al.*, this issue]. Below 200 m, isotherms within the eddy are displaced downward relative to surrounding waters, and this distortion of the large-scale field is still apparent at 1000 m. Above 200 m, isotherms are displaced upward so that the feature has a dome-like appearance centered at 200 m. The water within the eddy is highly spicy (warm and salty) relative to surrounding waters. On a 26 σ_θ density surface (about 200-m depth), the temperature within the eddy is 2°C warmer than surrounding isopycnal waters (Figure 4). The density anomaly of the eddy shows a doming and vertical extent similar to the temperature anomaly, although salinity compensation is obviously important. The warmer temperatures and higher salinities in the eddy are associated with lower oxygen (Figure 4) and higher values of nutrients [*Cornuelle et al.*, this issue]. Although one can find water with the same temperature and salinity characteristics either farther offshore or far to the south, the low oxygen identifies it unambiguously as water of equatorial origin, whose path northward is along the coast via the CUC. At the time of the survey, the CTD stations at the continental slope show a temperature anomaly of about 1°C, only half that seen in the eddy. Using averaged climatology, one has to go as far south as Point Conception ($\approx$ 36°N) to find water of the same characteristics as the eddy. However, winter CTD data (February 1981) from CODE taken near the continental margin off Point Arena ($\approx$ 39°N) match the T-S characteristics of the water found in the eddy [*Huyer et al.*, 1998] (Figure 4). This suggests that the CUC seasonally transports anomalously warm and salty water at least as as far north as Point Arena. A formation time in February at the coast and a westward propagation of 1-3 km day^{-1} [*Cornuelle et al.*, this issue] is consistent with observing the eddy 400 km offshore in May. The quasi-geostrophic model results [*Cornuelle et al.*, this issue] suggest a highly nonlinear eddy transporting anomalous water westward; the observations show that the anomaly is still very strong several months after the hypothesized generation. *Huyer et al.* [1998] document several anticyclones observed during summer 1993 between 36°N and 39°N and between the coast and 128°W, including two anticyclones that had anomalous water mass signatures. One of these, observed in June centered at 36°15'N, 125°30'W, had a subsurface lens at 150 m that was about 1°C warmer and 0.2 practical salinity unit (psu) saltier than surrounding waters. We do not think that the June and May eddies are the same, since the propagation in both cases is westward, and our observation site in May is further west (about 128°W). Also, the anomalies of the May eddy were stronger, although both sets of anomalies were consistent with CUC origins [*Huyer et al.*, 1998]. Subsurface floats deployed during EBC tracked numerous anticyclonic eddies originating in the CUC region during the same time period [*Garfield et al.*, 1999]. The hydrographic observations [*Huyer et al.*, 1998] that documented some of these anticyclones suggest that at least some of them trap CUC water and transport it offshore.

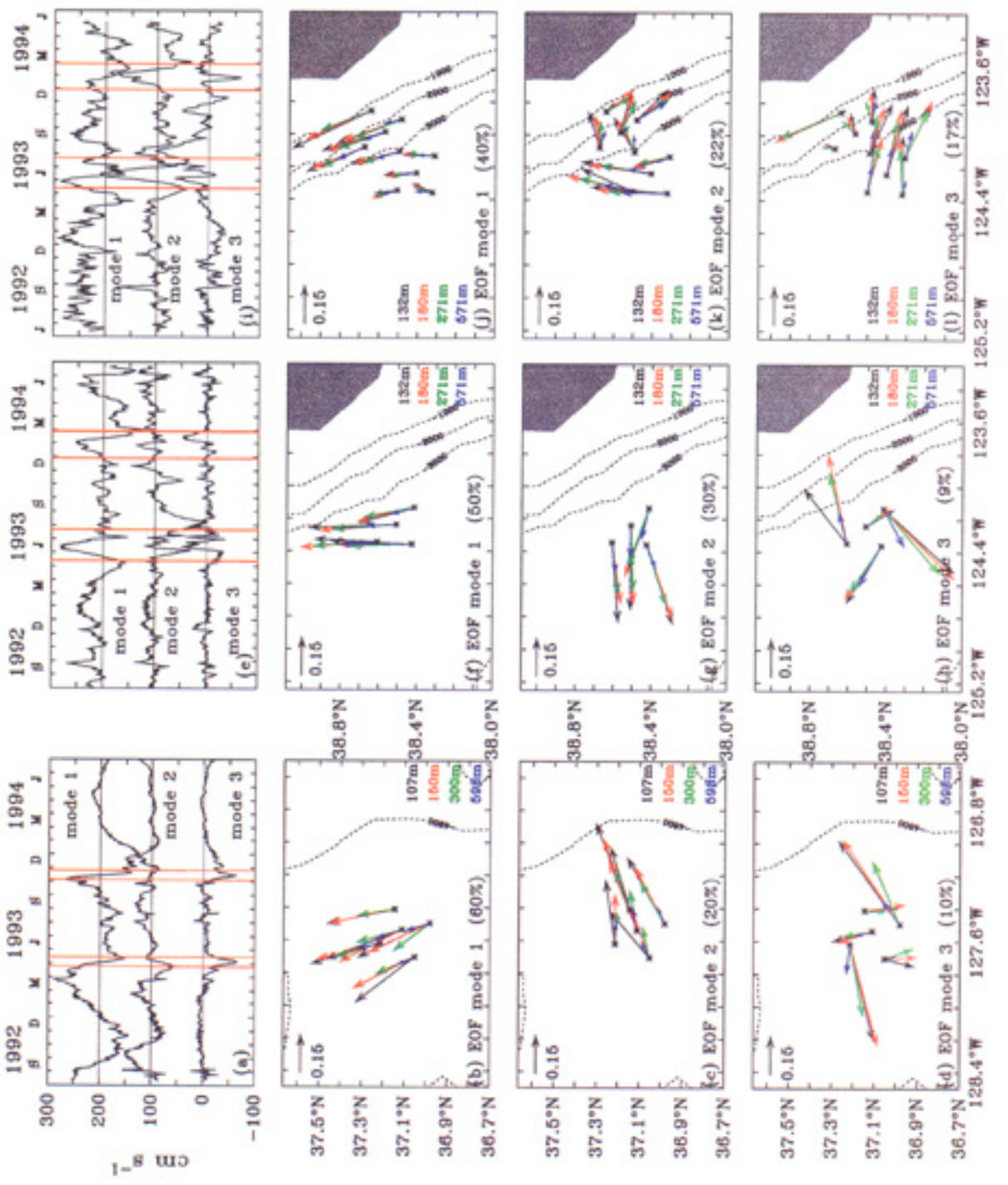

Plate 5. First three empirical orthogonal function (EOF) modes computed from velocity data for 2-year deployments, overlaid on bathymetry. Velocity depths are distinguished by the same colors as in Plate 2. The eddy event time periods noted on Plate 3 and Figure 1 are indicated on the temporal EOFs (Plates 5a, 5e, and 5i) by red vertical lines. Modes 1 and 2 temporal EOFs are offset by 200 and 100 cm s^{-1}, respectively. Percent variance explained by each mode is given in parentheses for the offshore LDA (Plates 5b-5d), inshore LDA (Plates 5f-5h), and the combined inshore and slope LDAs (Plates 5j-5l).

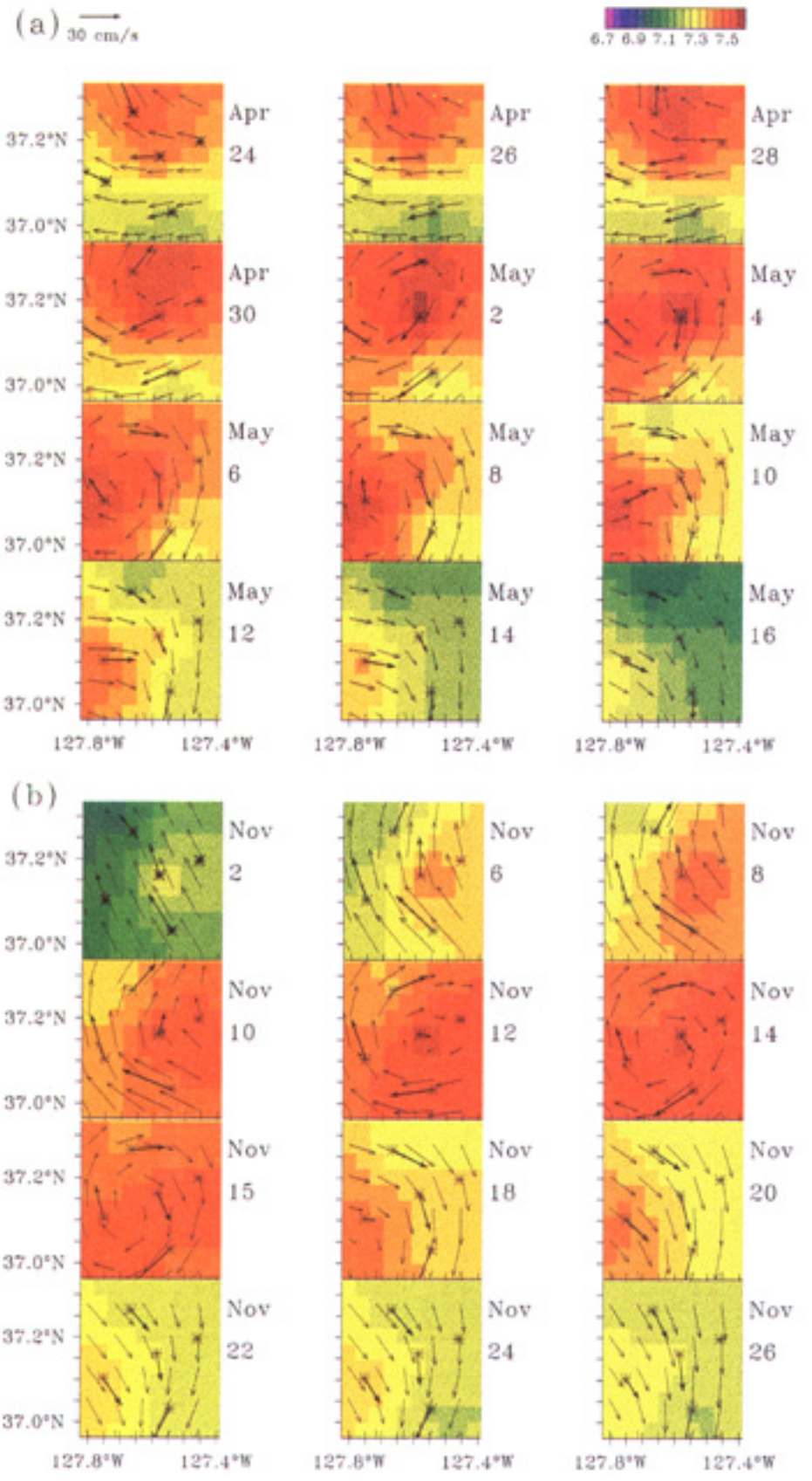

Plate 6. Objectively mapped temperature (color) and currents (arrows) during the passage of eddies through the offshore LDA in (a) May and (b) November 1993. Temperature is vertically averaged from 150 to 598 m, as a proxy for dynamic height, and velocity is at 107 m. Daily averaged moored velocities (bold arrows) are plotted at the mooring locations (asterisks). Velocity and temperature scales are shown in Plate 6a.

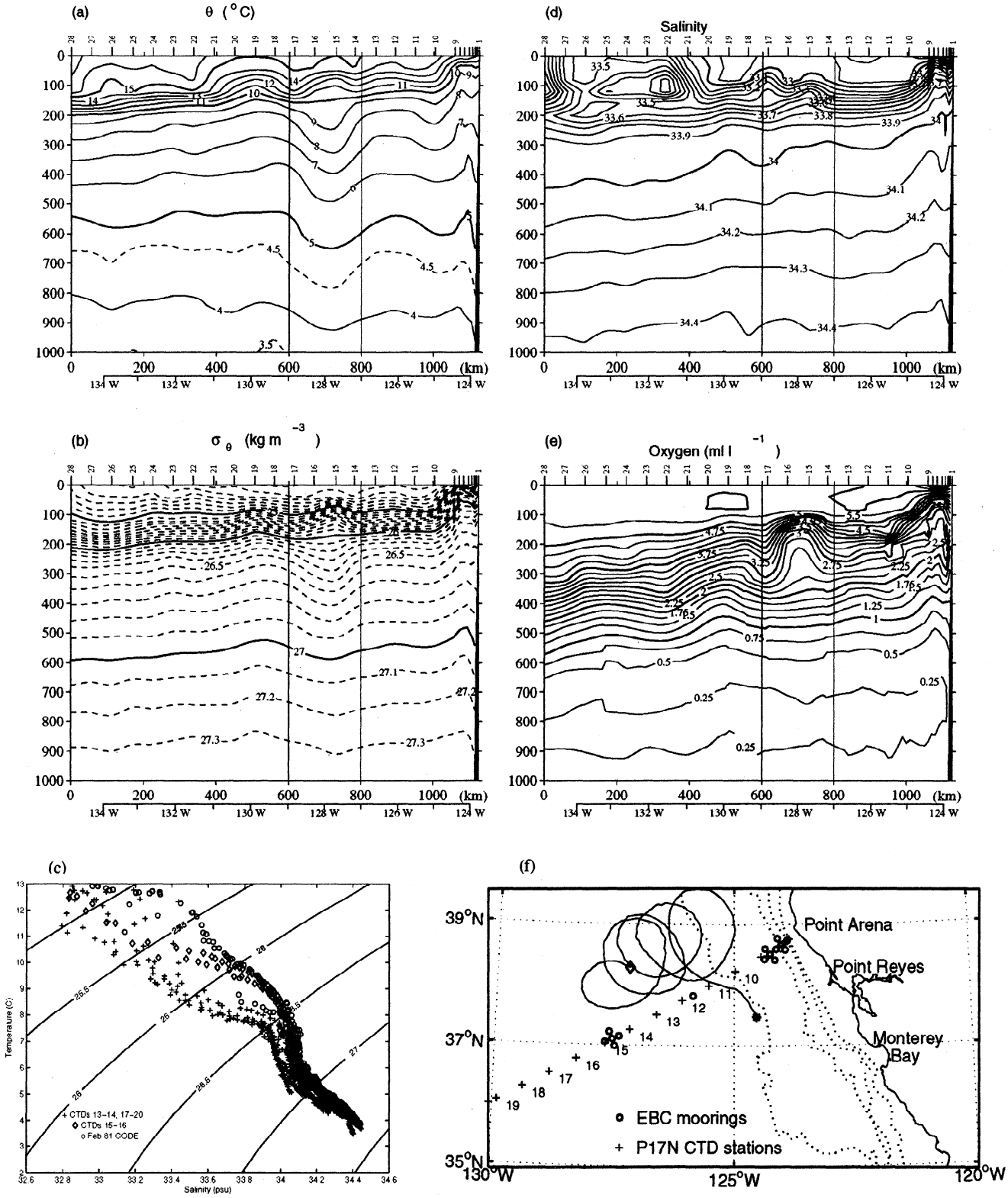

Figure 4. Vertical sections of potential temperature, salinity, oxygen, and σ_θ from the World Ocean Circulation Experiment (WOCE) P17N hydrographic survey that sampled past the offshore LDA on May 19, 1993. The May eddy is marked on property diagrams by vertical lines. The map indicates conductivity-temperature-depth (CTD) stations and mooring locations, together with a subsurface float track. The float was deployed on August 22, 1994 (asterisk); last position was on December 30, 1994 (diamond). The T-S diagram contrasts the eddy properties (casts 15 and 16) with those of the surrounding waters. The maximum temperature anomaly in the eddy is 2°C on the 26 σ_θ surface, at about 200 m. Water at the coast at the time of the survey does not show such a strong temperature anomaly (not shown). A similar anomaly is seen at the coast in winter data (February 1981) from the Coastal Ocean Dynamics Experiment (CODE).

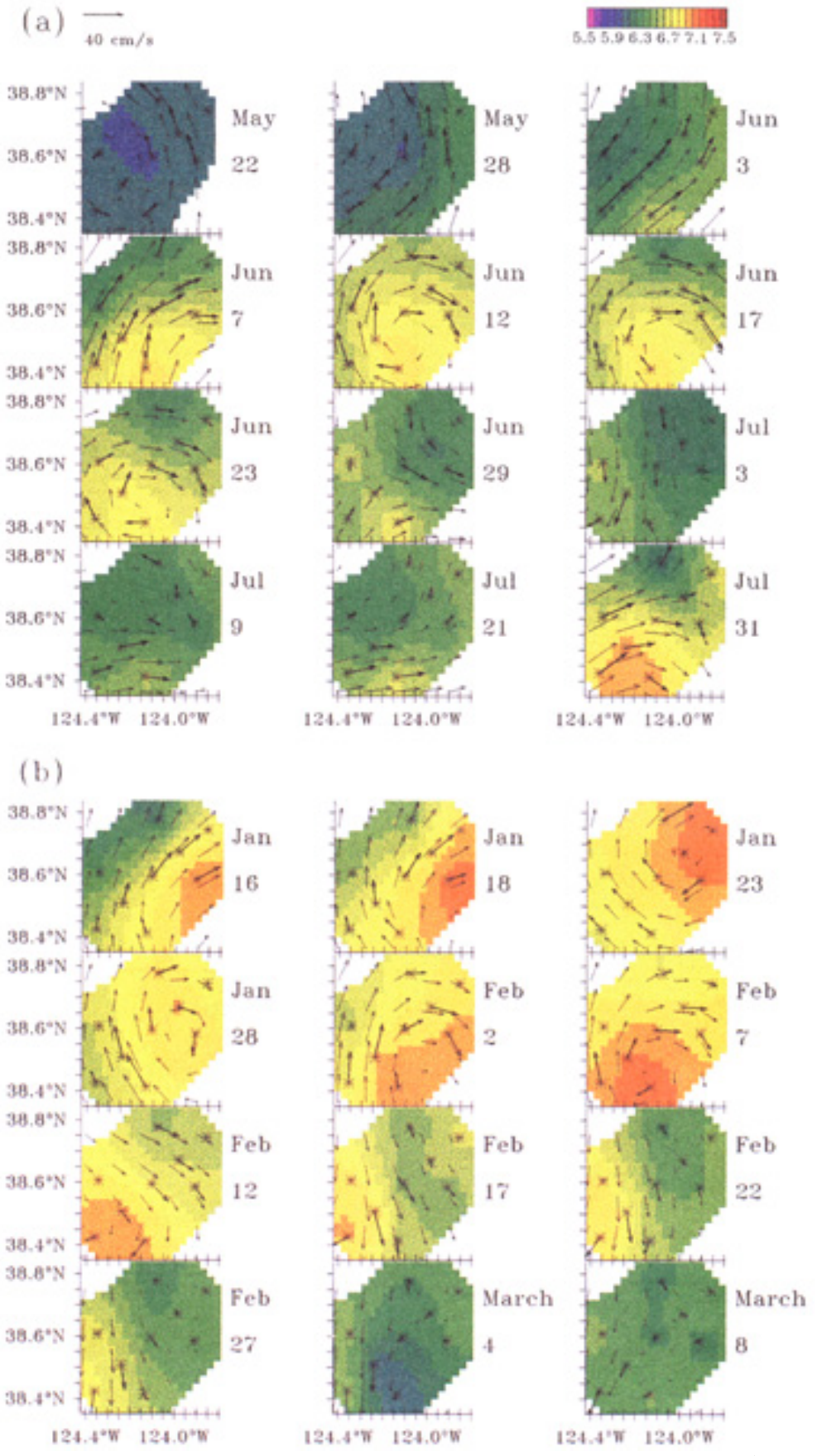

Plate 7. Objectively mapped temperature (color) and currents (arrows) during two large-amplitude eddy or meander events across the nearshore LDAs in (a) June-July 1993 and (b) January-February 1994. Temperature is vertically averaged from 180 to 571 m, as a proxy for dynamic height, and velocity is at 132 m. Daily averaged moored velocities (bold arrows) are plotted at the mooring locations (asterisks). Velocity and temperature scales are shown in Plate 7a.

Advanced very high resolution radiometer (AVHRR) images in this region typically show long squirts of cold upwelled water extending outward from the coast associated with fast velocity jets and an energetic eddy field. During the November eddy passage, the offshore tail of one such cold filament can be seen extending from 125°W toward the offshore array (Figure 5). Cold water patterns are consistent with a velocity field which rotates clockwise about the array. Slightly warmer sea surface temperatures (SSTs) are located to the east of the array. Comparison of the images from November 2 and 14 (Figure 5) suggests westward propagation of the anticyclonic feature which appears to be centered over the offshore array on November 14. Overcast conditions preclude the use of later AHVRR images to trace the evolution of this surface signature. Thermal images during the first eddy event (not shown) are not as conclusive, but there is also a suggestion of anticylonic flow on May 8 with a small finger of cold water encircling the array.

One additional occurrence of intensified flow and rapid change in flow direction (from southeastward to southwestward) occurred in early 1995 at the central offshore mooring. This velocity field is consistent with an anticyclonic eddy propagating westward with the eddy center located to the north of the array. Unfortunately, this cannot be checked with other nearby current meter records, as only one mooring was deployed from 1994 to 1996. However, a subsurface float track deployed between August 22 and December 30, 1994, supports this view. The float (at about 350-m depth) was caught in an anticyclonic eddy and had a motion radius of 71 km and a period of about 27 days [*Garfield et al.*, 1999]. The float moved westward from 124.5°W, 37.5°N in August to 127.2°W, 38.3°N at the end of December 1994. It surfaced to the east and north of the offshore array (Figure 4f).

To summarize, all evidence suggests that we have briefly sampled the center of two warm-core eddies as they propagated across the offshore array in May and November 1993. These eddies are characterized by small velocity divergence and large negative relative vorticity across the 50-km scale of the array. Temperature records indicate that eddies are associated with lower water column warming and concomitant cooling above 100 m. For the May eddy, a nearly simultaneous CTD section shows the upward/downward doming of isopycnals around the eddy center ($\sim$ 200 m) down to 1000 m. Water mass properties of the eddy measured by the hydrographic section indicate water of high spiciness that matched water of equatorial origin brought northward along the coast by the CUC during winter months [see also *Huyer et al.*, 1998]. This is strong support for a generation at the coast and propagation for several months over hundreds of kilometers with little dissipation.

5.2. Nearshore Events

Variability at the two nearshore arrays is more confused with several different patterns emerging over the 2-year period. EOF analysis calculated the dominant modes of variability which can be visually identified from the time series. Rather than describe all of the numerous patterns, we focus on the two intervals which are dramatically distinct with coherent variability across the combined inshore/slope array. During the two events, the evolution of velocity and temperature shares common features with the offshore eddy events. Plate 7 and Figure 6 are counterparts to the offshore array, but in this case they display data from the combined inshore/slope array. In Plate 7, temperature has been plotted only if the mapping error was $< 20\%$.

It is clear from the mapped temperature and velocity fields that these events are not straightforward westward propagat-

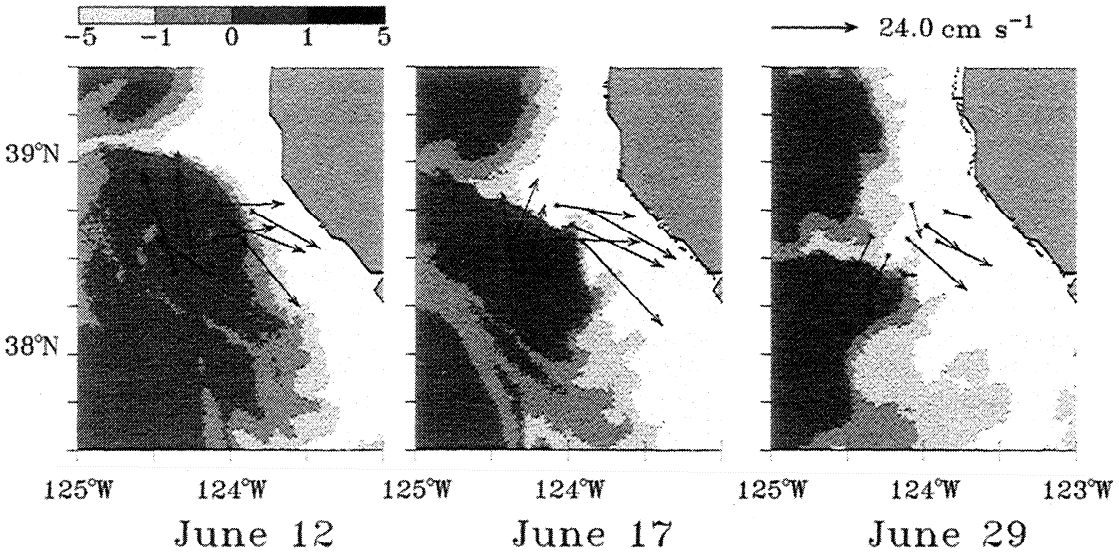

Figure 5. Velocity vectors at 107 m (sum of the first three EOFs) during the November 1993 passage of a deep, warm anticyclone at the offshore LDA, overlaid on advanced very high resolution radiometer (AVHRR) images. The area-averaged sea surface temperature (SST) has been removed from the AVHRR images; the gray scale refers to SST anomalies in °C, with cold anomalies colored light gray.

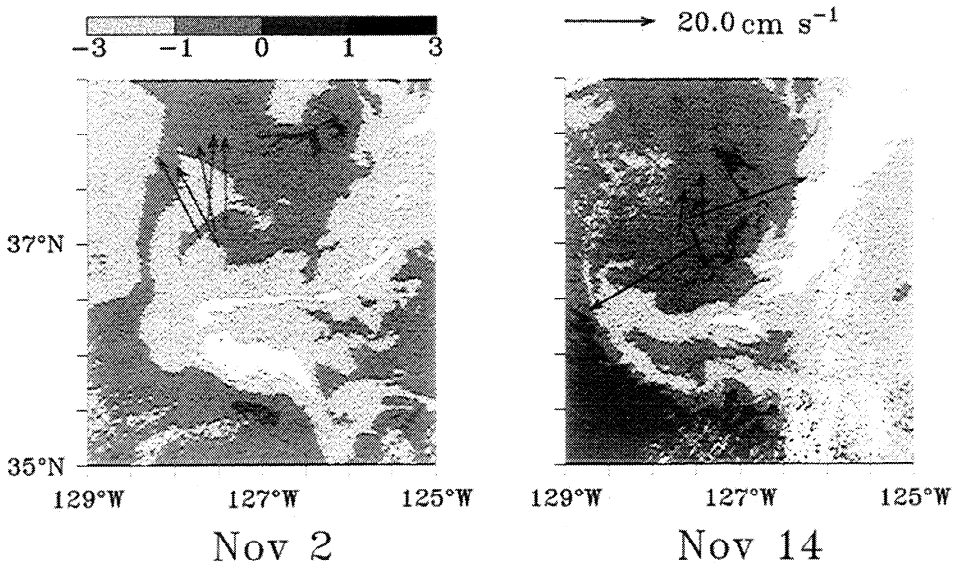

Figure 6. Velocity vectors at 132 m (sum of the first three EOFs) during the June 1993 passage of a warm anticyclone at the nearshore LDAs, overlaid on AVHRR images. The area-averaged sea surface temperature (SST) has been removed from the AVHRR images; the gray scale refers to SST anomalies in °C, with cold anomalies colored light gray.

ing eddies. We focus first on the selected interval from May 22 to July 31, 1993. A cyclonic feature with positive relative vorticity (Figure 1b) is apparent from May 22 to June 3 (Plate 7). Beginning with the June 3 map, a patch of warm water and associated anticyclonic flow appear to advect into the array from the southeast corner. The eddy was sampled for about 15 days, after which it was replaced by cool water and southward flow (July 3). The June time period coincided with a SeaSoar survey [*Huyer et al.*, 1998] which indicated that the moorings measured the northernmost of a series of eddies centered on the upper slope. A buildup of eastward velocity and cyclonic flow (July 9-21) precedes the arrival of another anticyclonic eddy from the south on July 31. This eddy covers only the southern part of the array, and relative vorticity estimated over the combined nearshore arrays remains positive (Figure 1b). Although not shown, the flow pattern remained virtually the same for a further 3 weeks, with intense onshore flow (high EOF 3 amplitudes). The feature appeared to be stable and did not propagate northward or westward across the array.

Fortunately, several clear AVHRR images were recorded during the summer of 1993. Traditionally, summer is a strong upwelling season associated with well-developed offshore squirts of cold water. Upwelled water pressed against the coast can be seen in the AVHRR maps in Figure 6. A thin filament of cold water extending seaward is present to the north of the arrays in June 12-17. Water temperatures are higher to the south, consistent with Plate 7. Strong offshore jets often occur along the northern edge of the cold filaments with shoreward return jets or eddies to the south [*Swenson et al.*, 1992]. Meridional temperature gradients are weakened as the cold water jets spread southward across the array, and temperatures are low when the filament is located over the array (June 29).

The strongest EOF signals of the eddies are in the second mode amplitudes which describe anticyclonic rotation and in an abrupt transition of northward to southward flow in EOF mode 1. These characteristics are shared with the offshore events. The difference between the inshore and offshore events is that eddy events at the inshore arrays do not propagate relatively quickly across the array but linger for periods of weeks over the combined array.

6. Conclusions

Moored observations of currents and temperatures made in the upper 600 m on eddy-resolving scales over a 2-year period provide an improved description, both qualitatively and quantitatively, of the California Current mesoscale circulation. As in prior studies [e.g., *Kosro et al.*, 1991], we observed that many eddies were generated over the outer continental slope. Furthermore, the good horizontal resolution of the current meter arrays allowed us to estimate the relative vorticity and the horizontal divergence from linear gradient estimates and therefore to evaluate the relative strength and occurrence of anticyclones and cyclones. These synoptic, two-dimensional, quantitative estimates from arrays that resolve the local Rossby deformation radius are new, and they reveal a mesoscale eddy field that is strongly nonlinear, with Rossby numbers ranging from 0.1 to 0.5. In fact, the large Rossby numbers imply that the curvature terms in the vorticity balance are nonnegligible, although our arrays are not adequate to resolve these higher-order terms. Both anticyclones and cyclones were observed at the nearshore arrays, although the anticyclones were somewhat stronger and of longer duration. The dominant 60-day period of the nearshore mesoscale circulation was well-resolved by the 2-year time series.

Prior to our measurements, there were no long-term time series in the outer CCS on eddy-resolving scales. The individual statistics of our offshore moorings confirmed the findings of earlier, widely separated moorings that showed that variability in the CCS far exceeded the mean flow [*Stabeno and Smith*, 1987]. Unlike the coastal zone, the outer CCS that we observed was not densely packed with eddies. The offshore mesoscale circulation had a peak at 120–180 days, not well-resolved by a 2-year time series. The offshore time series were dominated by a few event-like features (strong eddies) and a low-frequency variability that was not well-correlated with the large-scale wind stress curl, leading us to infer the importance of small-scale local wind forcing for the low-frequency background variability. Because of the event-like nature of the flow, particularly at the offshore site, we chose to look at patterns coherent across the arrays, through EOF analysis. Surprisingly, despite the distance from the coast and significant topography, the spatial modes of variability at the offshore array were nearly identical to those at the nearshore arrays, consisting of an alongshore mode, a cross-shore mode, and an eddy (rotational) mode. These three modes accounted for about 85% of the variance at all locations.

All of the eddies observed at the offshore array were deep, warm anticyclones, and they were highly nonlinear. Shipboard hydrography during the May eddy showed that it had trapped anomalous water from the California Undercurrent, suggesting a formation near the continental slope sometime during the previous winter. Model reconstruction of this eddy [*Cornuelle et al.*, this issue] suggests a Rossby number of O(1), underestimated by our finite difference calculation, and supports an interpretation of it as a submesoscale coherent vortex. Prior, isolated observations have been made of Undercurrent eddies near the coast, for example, near Point Conception [*Simpson and Lynn*, 1990] and Point Arena [*Kosro et al.*, 1991]. The EBC observations from moorings, surveys [*Huyer et al.*, 1998], and floats [*Garfield et al.*, 1999] documented numerous instances of these CUC eddies at points further offshore than previously observed, which suggests they are not rare anomalies in the CCS, but are ubiquitous. Their subsurface maxima in both currents and hydrography suggest that they may be underrepresented in remote-sensing and surface drifter measurements. Our offshore moored observations indicate that CUC eddies, in addition to being highly nonlinear, are also stable and robust [*Cornuelle et al.*, this issue] and are capable of transporting fluid and properties at least 400 km offshore, orthogonal to the meridionally oriented mean flow of the CCS. These eddies may provide a principal means of transport and exchange of properties between the coast and the central North Pacific Ocean.

Appendix A: Mooring Deployments

A1. Offshore LDA

The Rosenstiel School of Marine and Atmospheric Sciences (RSMAS) Technical Services Group was responsible for instrument deployment and initial data processing at the offshore LDA (array code O). A combination of vector-averaging current meters (VACMs) and Aanderaa current meters (ACMs) was used. The VACMs had a 30-min averaging interval and recording rate. With an averaging period of 30 min and a current speed of 10 cm s^{-1}, the compass and vane follower would be sampled about 4000 times and vector averaged. VACM temperature and pressure were also averaged over that interval. Vector-averaging Aanderaas (RCM8s) sampled the compass and generated a vector $\sim$ 100 times over the averaging interval of 2 hours. At the end of the averaging interval, the current as well as instantaneous temperature and pressure were recorded. Aanderaa RCM5s recorded the accumulated rotor counts as well as instantaneous current direction; temperature and pressure were recorded every 3 hours. The central mooring is an exception with VACMs at all four levels; additionally, an RCM5 was placed 1 m below the VACM at 600 m for the purpose of comparing instruments. RSMAS was also responsible for the single mooring (code IOC) located near 126°W, which had RCM5s at three levels. The central offshore mooring was redeployed in August 1994 in order to maintain the current measurements and a sound source array [*Garfield et al.*, 1999] for an additional 2 years. Aanderaa RCM8s with a 2-hour recording interval were placed at each depth. Mooring OE accidentally released in April 1993 and was not redeployed.

A2. Inshore LDA

The four moorings at the inshore LDA (array code I) were deployed by the Woods Hole Oceanographic Institution (WHOI) current meter facility. The current meters were all VACMs with an averaging interval and recording rate of 15 min. The IN mooring accidentally released in March 1993 and was reset again a month later, resulting in a data gap. The deepest current meter on the IW mooring gave less than $< 50\%$ data return with bad sections at the beginning and middle of the record.

A3. Slope LDA

The five moorings at the slope array (array code M) were deployed by the Naval Postgraduate School (NPS) current meter group. There were two consecutive year-long deployments. Aanderaa RCM8s, with averaging and recording intervals of 1 hour, were used at all depths for the first deployment. In the second deployment, the shallowest RCM8s were replaced with upward looking 300 kHz acoustic Doppler current profilers (ADCPs) at a nominal depth of 150 m. The bin size for the ADCP measurements was 4 m with a nominal total number of 45 bins. Pressure-depth recorders at nearly all instruments provided pressure and temperature time series. ADCP velocity data from the bin corresponding to the shallowest common depth (132 m) was extracted for the purposes of this analysis. The shallowest ACM at MC was placed above 132 m so the ACM-derived velocities and temperatures were used in place of the ADCP data. The ME ADCP leaked, so there is no shallow record after May 1993.

Appendix B: Gradient Estimation

Conceptually, velocity at a fixed depth level z_l at mooring i within an LDA can be expanded in a Taylor series relative to the array center (x_c, y_c, z_l, t):

$$u_i = u_c(x_c, y_c, z_l, t) + \frac{\partial u}{\partial x}\Delta x_i + \frac{\partial u}{\partial y}\Delta y_i + ..., \quad \text{(B1)}$$

where u_i is the eastward velocity at mooring i, (Δx_i, Δy_i) are the distances from mooring i to the array center, and (u_c, $\partial u/\partial x$, $\partial u/\partial y$) are the model parameters to be estimated at each time t at the array center. Northward velocity is treated similarly.

For n moorings, the problem to be solved for the three unknowns at each time t is written as a linear matrix equation:

$$\mathbf{d} = A\mathbf{m} + \mathbf{r}, \quad \text{(B2)}$$

where $\mathbf{d}$ is the nx1 vector of observations, A is the nx3 coefficient matrix for the Taylor expansion, $\mathbf{m}$ is the 3x1 vector of unknowns, and $\mathbf{r}$ is an nx1 residual vector. The residual results both from errors in the observations and from the inadequacy of the model (i.e., neglect of higher-order terms in the Taylor expansion). We specified model and residual covariance matrices P and R, respectively. P is a diagonal matrix specifying the expected signal variance in the model parameters $\mathbf{m}$. These variances were estimated from the current meter statistics (Table 2) and were kept constant for all t. R is a diagonal matrix specifying the expected residual variance. The residual variance was set at 20% of the signal variance for the offshore array and 30% of the signal variance for the nearshore arrays. The increased residual variance for the nearshore arrays reflects an increase in expected model misfit in estimating linear gradients across two arrays. There are two equivalent forms for the solution [*Liebelt*, 1967]:

$$\hat{\mathbf{m}} = PA'[APA' + R]^{-1}\mathbf{d} \quad \text{(B3)}$$

$$\hat{\mathbf{m}} = [P^{-1} + A'R^{-1}A]^{-1}A'R^{-1}\mathbf{d}, \quad \text{(B4)}$$

where prime denotes matrix transpose. Note that P^{-1} and R^{-1} are trivial inverses to compute since they are diagonal matrices. We solved the overdetermined (B4) form, which required computing a 3x3 inverse at each time t. The uncertainty variance in the model parameter estimates is given by

$$\hat{P} = P^{-1} + A'R^{-1}A. \quad \text{(B5)}$$

Note that the uncertainty depends on the assumed covariance matrices as well as on the array geometry. In particular, the uncertainties increase as the number of moorings decrease; hence we chose to present the most complete depth level in Figure 1. Uncertainties in vorticity and divergence were computed as for the sum of two independent random variables since they are each the sum of two orthogonal gradient terms. As a consistency check, we monitored the velocity residuals normalized by the square root of the expected residual variance and the calculated model parameters normalized by the square root of the expected model variance. The distribution of these normalized quantities was consistent with a Gaussian distribution, that is, < 1 for 90% of the 2-year time interval, a small percentage of outliers, and no extreme outliers.

Acknowledgments. The Eastern Boundary Currents California Current moored array was funded by the Office of Naval Research as part of the ONR Accelerated Research Initiative on interactions in nonlinear mesoscale regimes. The P17N hydrographic section was funded by the National Science Foundation as part of the World Ocean Circulation Experiment. PCM2 data can be obtained from the WOCE current meter data assembly center (http://-cmdac.oce.orst.edu). P17N hydrographic data can be obtained from the WOCE Hydrographic Office (http://whpo.ucsd.edu). We gratefully acknowledge support from the following grants: N000-14-92-J-1584 and OCE-9216411 (T.K.C. and M.Y.M.), N00014-91-J-1016 and N00014-98-1-0024 (P.P.N. and T.K.C.), N00014-92J1357 and N00014-98-1-0026 (P.M.K. and R.L.S.), and OCE-9106472 (D.L.M.). C.A.C. and S.R.R. were supported by ONR and the Oceanographer of the Navy. The manuscript benefited from discussions with Bruce Cornuelle, Alistair Harding, and Jane Huyer.

References

Chelton, D. B., A. W. Bratkovich, R. L. Bernstein, and P. M. Kosro, Poleward flow off central California during spring and summer of 1981 and 1984, *J. Geophys. Res.*, *93*, 10,604–10,620, 1988.

Chereskin, T. K., Direct evidence for an Ekman balance in the California Current, *J. Geophys. Res.*, *100*, 18,261–18,269, 1995.

Collins, C. A., N. Garfield, R. G. Paquette, and E. Carter, Lagrangian measurement of subsurface poleward flow between 38°N and 43°N along the west coast of the United States during summer, 1993, *Geophys. Res. Lett.*, *23*, 2461–2464, 1996.

Cornuelle, B. D., T. K. Chereskin, P. P. Niiler, M. Y. Morris, and D. Musgrave, Observations and modeling of a California Undercurrent eddy, *J. Geophys. Res.*, this issue.

Davis, R. E., Predictability of sea surface temperature and sea level pressure anomalies of the North Pacific, *J. Phys. Oceanogr.*, *6*, 249–266, 1976.

Garfield, N., C. A. Collins, R. G. Paquette, and E. Carter, Lagrangian exploration of the California Undercurrent, 1992-1995, *J. Phys. Oceanogr.*, *29*, 560–583, 1999.

Hansen, D. V., and P-M. Poulain, Quality control and interpolations of WOCE/TOGA drifter data, *J. Atmos. Oceanic Technol.*, *13*, 900–909, 1996.

Hickey, B. M., The California Current system - Hypothesis and facts, *Prog. Oceanogr.*, *8*, 191–279, 1979.

Huyer, A., J. A. Barth, P. M. Kosro, R. K. Shearman, and R. L. Smith, Upper-ocean water mass characteristics of the California current, summer 1993, *Deep Sea Res., Part II*, *45*, 1411–1442, 1998.

Kelly, K. A., R. C. Beardsley, R. Limeburner, K. H. Brink, J. D. Paduan, and T. K. Chereskin, Variability of the near-surface eddy kinetic energy in the California Current based on altimetric, drifter, and moored current data, *J. Geophys. Res.*, *103*, 13,067–13,084, 1998.

Kosro, P. M., et al., The structure of the transition zone between coastal waters and the open ocean off northern California, winter and spring 1987, *J. Geophys. Res.*, *96*, 14,707–14,730, 1991.

Kosro, P. M., S. R. Ramp, and R. L. Smith, Moored current measurements over the continental slope in EBC: A first look, *Eos Trans. AGU*, *75*(44), Fall Meet. Suppl., 345, 1994.

Largier, J., B. A. Magnell, and C. D. Winant, Subtidal circulation over the northern California shelf, *J. Geophys. Res.*, *98*, 18,147–18,179, 1993.

Liebelt, P. B., *An Introduction to Optimal Estimation*, 273 pp., Addison-Wesley, Reading, Mass., 1967.

Lorenz, E. N., Empirical orthogonal functions and statistical weather

prediction, *Sci. Rep. 1*, 49 pp., Stat. Forecast Proj., Mass. Inst. of Technol., Cambridge, Mass, 1956.

Lynn, R. J., and J. J. Simpson, The California Current System: The seasonal variability of its physical characteristics, *J. Geophys. Res.*, *92*, 12,974–12,966, 1987.

Musgrave, D. L., and T. C. Royer, P17N: A WHP section in the Northeast Pacific, *Eos Trans. AGU*, *75*(3), Ocean Sci. Meet. Suppl., 205, 1994.

Niiler, P. P., J. Filloux, W. T. Liu, R. M. Samelson, J. D. Paduan, and C. A. Paulson, Wind-forced variability of the deep eastern North Pacific: Observations of seafloor pressure and abyssal currents, *J. Geophys. Res.*, *98*, 22,589–22,602, 1993.

Priesendorfer, R. W., *Principal Component Analysis in Meteorology and Oceanography*, 425 pp., Elsevier Sci., New York, 1988.

Ramp, S. R., P. M. Kosro, R. L. Smith, and P. F. Jessen, The EBC-ARI slope array: Results from year 1, *Eos Trans. AGU*, *75*(3), Ocean Sci. Meet. Suppl., 140, 1994.

Ramp, S. R., L. K. Rosenfeld, T. D. Tisch, and M. R. Hicks, Moored observations of the current and temperature structure over the continental slope off central California, 1, A basic description of the variability, *J. Geophys. Res.*, *102*, 22,877–22,902, 1997.

Rienecker, M. M., and C. N. K. Mooers, A summary of the OPTOMA program's mesoscale ocean prediction studies in the California Current system, in *Mesoscale/Synoptic Coherent Structures in Geophysical Turbulence*, edited by J. C. J. Nihoul and B. M. Jamart, pp. 519–548, Elsevier Sci., New York, 1989.

Rienecker, M. M., C. N. K. Mooers, and R. L. Smith, Mesoscale variability in current meter measurements in the California Current system off northern California, *J. Geophys. Res.*, *93*, 6711–6734, 1988.

Shearman, R. K., J. A. Barth, and P. M. Kosro, Diagnosis of the three-dimensional circulation associated with mesoscale motion in the California Current, *J. Phys. Oceanogr.*, *29*, 651–670, 1999.

Simpson, J. J., and R. J. Lynn, A mesoscale eddy dipole in the offshore California Current, *J. Geophys. Res.*, *95*, 13,009–13,022, 1990.

Stabeno, P. J., and R. L. Smith, Deep-sea currents off northern California, *J. Geophys. Res.*, *92*, 755–771, 1987.

Strub, P. T., T. K. Chereskin, P. P. Niiler, C. James, and M. D. Levine, Altimeter-derived variability of surface velocities in the California Current System, 1, Evaluation of TOPEX altimeter velocity resolution, *J. Geophys. Res.*, *102*, 12,727–12,748, 1997.

Strub, P. T., and C. James, Altimeter-derived variability of surface velocities in the California Current System, 2, Seasonal circulation and eddy statistics, *Deep Sea Res., Part II*, in press, 1999.

Swenson, M. S., P. P. Niiler, K. H. Brink, and M. R. Abbott, Drifter observations of a cold filament off Point Arena, California, in July 1988, *J. Geophys. Res.*, *97*, 3593–3610, 1992.

Walstad, L. J., J. S. Allen, P. M. Kosro, and A. Huyer, Dynamics of the coastal transition zone through data assimilation studies, *J. Geophys. Res.*, *96*, 14,959–14,977, 1991.

Winant, C. D., R. C. Beardsley, and R. E. Davis, Moored wind, temperature, and current observations made during Coastal Ocean Dynamics Experiments 1 and 2 over the northern California continental shelf and upper slope, *J. Geophys. Res.*, *92*, 1569–1604, 1987.

Wyllie, J. G., Geostrophic flow of the California Current at the surface and at 200 m, *Atlas 4*, Calif. Coop. Oceanic Fish. Invest., La Jolla, Calif., 1966.

T. K. Chereskin and P. P. Niiler, Scripps Institution of Oceanography, University of California-San Diego, La Jolla, CA 92093-0230. (tchereskin@ucsd.edu; pniiler@ucsd.edu)

C. A. Collins and S. R. Ramp, Department of Oceanography, Naval Postgraduate School, 833 Dyer Road, Room 328, Monterey, CA 93943-5122. (collins@oc.nps.navy.mil; ramp@oc.nps.navy.mil)

P. M. Kosro and R. L. Smith, College of Oceanic and Atmospheric Sciences, Oceanography Admin. Bldg. 104, Oregon State University, Corvallis, OR 97331. (kosro@oce.orst.edu; rsmith@oce.orst.edu)

M. Y. Morris, National Institute of Water and Atmospheric Research Ltd., 301 Evans Bay Parade, Greta Point, P.O. Box 14-901, Kilbirnie, Wellington, New Zealand. (m.morris@niwa.cri.nz)

D. L. Musgrave, Institute of Marine Science, University of Alaska, Fairbanks, AK 99775. (musgrave@ims.alaska.edu)

(Received October 22, 1998; revised June 21, 1999;
accepted July 22, 1999.)